MASTER'S THESIS

Assessing the Role of Overturning and Remineralisation on Nitrate and Oxygen Distribution in a Global Ocean Model

Author:

Joseph Lartey

Matriculation Number:

3031508

Reviewers

Prof. Dr. Monika Rhein

Dr. Christoph Völker

Supervised by

Dr. Christoph Völker

Submitted to:

Institute of Environmental Physics and Remote Sensing (IUP - IFE)

University of Bremen, Bremen, Germany

In partial fulfilment of the requirement for the degree of master of science in environmental physics

March 7, 2019

Declaration of the Master Thesis

I, Joseph Lartey, hereby declare that this thesis was composed by myself, that the work contained herein is my own and did not use any other sources and auxiliary means than those indicated. I also give authorization for this work to become part of the permanent collection of the university archive.

Place, Date

Signature

Acknowledgement

I am very grateful to the almighty God for giving me life, understanding, wisdom, knowledge and the spirit of perseverance to successfully complete this thesis.

This thesis would not have been possible without my close association with many people who were always available when I needed them the most. I would like to acknowledge them and extend my sincere gratitude for helping me make this master thesis a possibility.

I would like to thank my supervisor Dr. Christoph Völker for the opportunity given me and also for his support, guidance, faith, patience, motivation, enthusiasm, encouragement, immense knowledge and selfless dedication during my work at the Alfred Wegener Institute for Polar and Marine Research (AWI).

I would also like to thank Prof. Dr. Monika Rhein for her guidance and support throughout the course of this research work.

My sincere thanks to Dr. Emmanuel Kwasi Addai, Dr. Essowe Panassa, Razib Vhuiyan and Sarpong Yaw Frimpong for their intellectual contribution and friendly motivation throughout the thesis period and my development as a student and researcher.

I would also like to express my very profound gratitude to my parent the late Mr. Patrick Afari Lartey and Ms. Elizabeth Adade Boateng and family members for providing me continuous encouragement and unfailing support throughout my study.

I wish to express my appreciation to Ms. Joyce Darko, Ms. Natalia Lartey Darko and my son Mr. Jaden-Allen Lartey for their motivation, encouragement, cheerful smile and devoted love which is my greatest source of human inspiration.

Dedication

I dedicate this work to my late father, Mr. Patrick Afari Lartey for his many sacrifices and encouragement. I would also like to dedicate this to my mother Elizabeth Adade Boateng, senior brother Dr. Emmanuel Lartey and my great uncle Mr. Peter Charmant, Natalia Lartey Darko, my son Jaden-Allen Lartey and my entire family for what they have done for me to reach this far .

Abstract

The distribution of dissolved inorganic nutrients and oxygen in the ocean is determined by their concentration in the main deep water mass formation regions, transport and mixing through deep ocean overturning circulation and remineralisation of organic matter by bacteria which releases inorganic nutrients and reduces oxygen. The nutrient distribution therefore reflects both the composition of water masses and water mass age. Imperfections of how the formation and spreading of water masses are represented in the ocean circulation models is directly reflected in the modelled nutrient and oxygen distributions. Here the global set-up of the version-2 of the Regulated Ecosystem Model (REcoM-2) was used and how well the distributions are represented in the REcoM-2 was analysed. The model is initialised with the temperature, salinity, oxygen and inorganic nutrient from the World Ocean Atlas 2009, (WOA09) and is integrated over 1000 years under a monthly, annual and seasonal climatological forcing. The model produced an output that shows some deviations from the output of the observational WOA09. The model produces a deep ocean that is too warm and salty in both the Atlantic and Pacific Oceans, a common feature in low-resolution models. The deep Atlantic and Pacific are also depleted in nutrients and have extremely high oxygen concentration except in the Southern Ocean. A number of sensitivity runs were performed with the model to determine whether these biases can be attributed to the modelled physical circulation or the representation of the biological pump.

The modification of the model physics enhanced the representation of the overturning circulation in the model. Shallowing the topography in the Denmark Strait made the overturning circulation more realistic with a magnitude of $21.8 Sv$ across 24°N compared with $23.3 Sv$ from the standard model. This also improved the fit to the nitrate and oxygen distribution.

Changes in the biogeochemistry also show clear improvement in the nitrate fields in terms of the biases, correlation and the root mean squared difference (RMSD) of the sensitivity experiments. The biases of the dissolved inorganic nitrate and oxygen were decreased and their correlation was increased. The RMSD was reduced when the vertical gradient of the sinking speed was increased and increased when the carbon and nitrogen remineralisation rate was decreased.

Contents

List of Figures

List of Tables

Chapter 1

Introduction

1.1 Motivation

The distribution of dissolved nutrients such as nitrogen, phosphorous, silicon, and iron in the ocean is an important factor in determining its biological productivity. At the same time, the distribution of nutrients is influenced both by transport and mixing through the circulation of the ocean and by the action of biology. Through the production of chemical compounds by living organisms, these elements are converted into different types of organic matter for cellular growth, metabolism, and structure such as the amino acids built from proteins, nucleic acids, and phospholipids membranes.

On the other hand, the nutrients are regenerated by the breakdown of organic matter when it is consumed by animals or bacteria. Production of new biomass and uptake of nutrients in the ocean tend to happen near the surface because of the availability of light, but regeneration occurs all through the water column. Because of that, the surface water is typically depleted in nutrients except for high latitudes and upwelling zones. The transport of nutrients back to the surface is done by vertical mixing and upwelling. The uptake of nutrients by plants or phytoplankton is connected with the release of oxygen through photosynthesis and regeneration of nutrients by bacteria production or animal consumption is connected with the use of oxygen.

All these processes have to be represented in global ocean biogeochemistry models to reproduce realistic distributions of nutrients and oxygen. Doing so is a prerequisite for modelling a realistic distribution of biological ocean productivity and the global carbon cycle. But the ocean models, both physical and biogeochemical are never perfect. They have biases in how they reproduce circulation and the distribution of biological activity. The purpose of this thesis is to investigate how well the distribution of nutrients and oxygen is represented in a global set-up of the REcoM- 2 model. And should there be larger deviations between the model-produced nutrient fields and observation, attention will be drawn to the cause being the modelled physical circulation or the representation of the biological pump through a number of sensitivity runs with the model.

1.2 Nutrient and oxygen distribution in the ocean

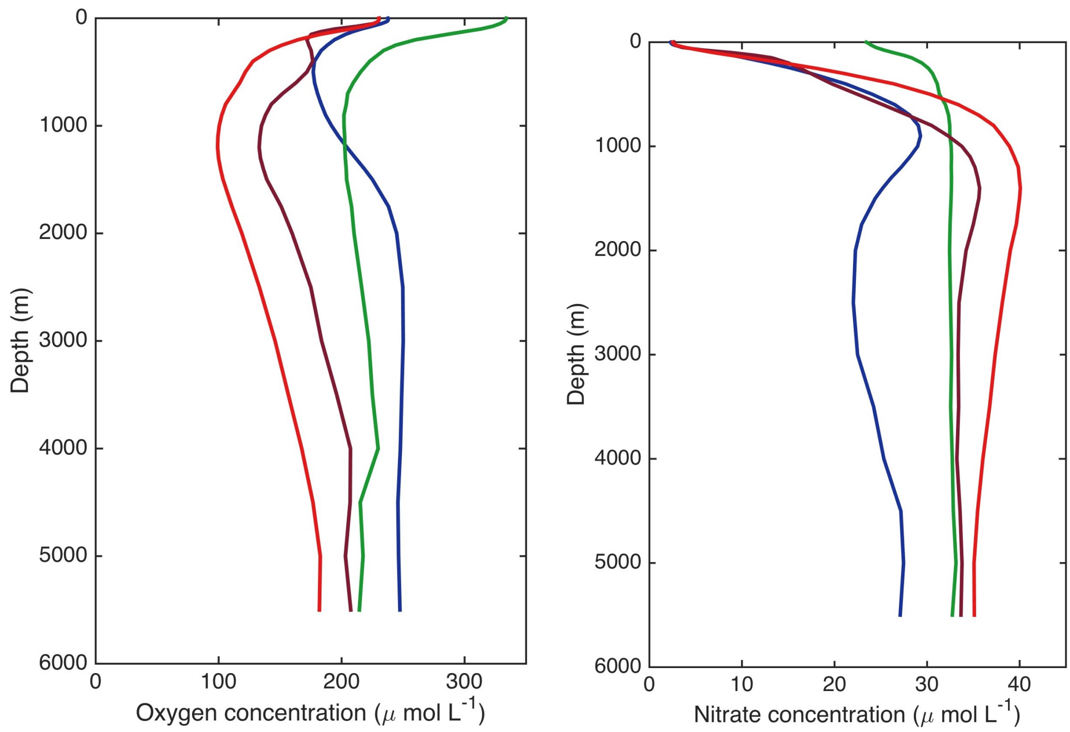

Figure 1.1: *Average vertical profile of the the distribution of nitrate and oxygen in the ocean basins [Atlantic (Blue), Southern (Green), Indian (Violet) and Pacific (Red)]*

.

In general, nutrients have a minimum concentration at the surface, a maximum at mid-depth and decrease gradually with depth below maximum. A typical example is the distribution of nitrate in the different ocean basins as shown in Figure 1.1. Nitrate in the Atlantic for instance, increases with depth but slightly decreases from about $1000m$ till about $2700m$ where the concentration begins to stabilise to the abyss of the ocean. Oxygen on the other hand often decreases with depth but increases again in the deep cold water masses below about $800m$ depth.

The nutrient distribution in the ocean is primarily controlled by the production in surface waters, remineralisation of organic matter by bacteria, the sinking of particulate organic matter and by advection with the deep ocean circulation

(Hirose & Kamiya 2003). The nutrient distribution is coupled to that of dissolved oxygen since photosynthesis releases oxygen and respiration requires oxygen. Nutrients in the deep ocean increase with water mass age: Highest values are found in the deep North Pacific, lower values in freshly ventilated deep North Atlantic. Oxygen which is produced during photosynthesis but used during remineralisation should follow the opposite pattern. But for oxygen, another factor is the solubility of O_2 in seawater which is higher in colder water. The production of organic matter by photosynthesis is restricted to the upper sunlit surface water, whilst respiration occurs in every part of the water column (Sigman & Haug 2003). Nutrients are depleted near the surface due to photosynthesis and increase where there is respiration. Respiration leads to the loss of oxygen in the ocean, in some places leading to the formation of an oxygen minimum zone under high-productivity upwelling regions.

1.3 The biological pump

Because organic matter also contains carbon in addition to nitrogen and other nutrients, the cycling of nutrients is also connected to that of carbon. Volk & Hoffert (1985) defined carbon pumps as the processes that exhaust the ocean surface of carbon dioxide. By drawing down CO_2, these pumps influence the equilibrium between the carbon at the ocean surface and the atmospheric CO_2. The biological pump is responsible for both vertical and horizontal differences in the concentration of nutrients.

The net effect of the biological carbon pump is to transport carbon from the upper ocean to the deep ocean. The relative proportion of the elements in the organic matter is described by the Redfield ratio. This ratio affects the cycling of nutrients in the ocean since their relative proportion relates the utilisation of different nutrients and also couples to the distribution of carbon and oxygen since there is a constant O_2: C ratio. The classical P:N:C:O_2 ratio based on the study of phytoplankton decomposition is 1:16:106:-138 (Anderson & Sarmiento 1994). All the values are relative to the phosphorus value. Several studies have slightly modified this ratio to 1: 16$\pm$1: 117$\pm$14: -170$\pm$10 by Anderson & Sarmiento (1994), 1:16:106:-141 to -161 by Anderson (1995), 1:17.5$\pm$2:123$\pm$10:-165$\pm$15 by Körtzinger et al. (2001) and 1:17:106:-154 by Hedges et al. (2002) based on co-variation of nutrients in the ocean as in the composition of organic matter.

Since uptake and release of carbon are thus always coupled to changes in nitrogen, phosphorus, and oxygen, the concentrations of dissolved inorganic carbon

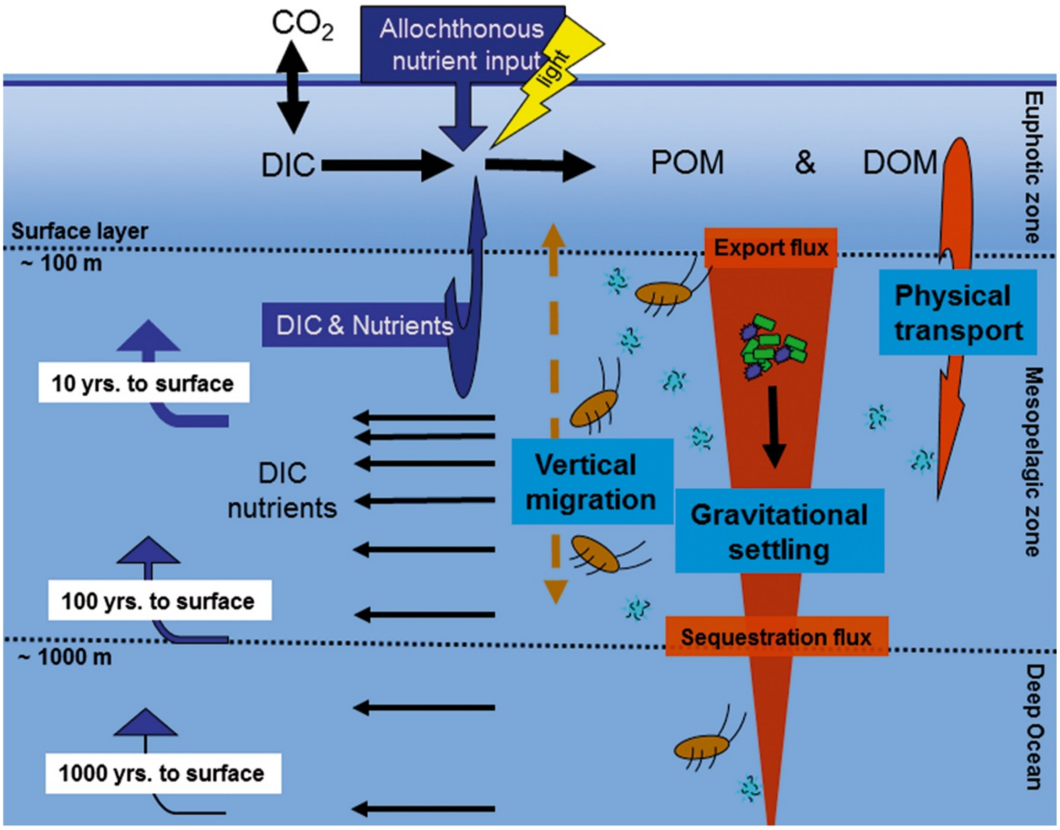

Figure 1.2: *Description of the biological pump. The organic matter in the sunlit zone is transported to depth by the gravitational settling, physical transport of the dissolved organic matter (DOM) and the vertical movement of the zooplankton(brown ovals with antennas), gravitational settling of marine snow (green clusters with black bacteria) or physical transport of dissolved organic matter (DOM). The sinking flux is reduced with depth due to the remineralisation of the organic matter (symbolized by green cells and blue transparent exopolymer particles). Both the depth of remineralisation and the timescale of oceanic transport determines the time that it takes for the DIC and DIN to return to the surface. From (Passow & Carlson 2012)*

.

(DIC), dissolved inorganic nitrogen (DIN), PO_4^{3-}, O_2 often co-vary. This is most evident for NO_3^{2-} and PO_4^{3-}, while DIC and O_2 also exchange with the atmosphere making their relation to nitrate and phosphate complicated.

The biological pump can be separated into several steps including the production of organic matter and biominerals at the surface, sinking of particles into deeper ocean and the decomposition of the settled particle as shown in Figure 1.2.

Phytoplankton transfers and take up the dissolved nutrients and carbon into particulate organic matter (POM) and biominerals to form new biomass near the sunlit water surface through photosynthesis. The biomass produced by phytoplankton is used by other organisms from bacteria to whales, and forms the basis of the marine food web. Nutrients are completely taken up by phytoplankton in most of the low and mid-latitudes.

This is followed by the subsequent sinking of these particles produced by the phytoplankton. Not all of these particles and biominerals are decomposed by dissolution which, decreases the sinking flux of the particles by zooplankton grazing and the decomposition of sinking and suspended particles by hydrolysis at the surface but huge amount are able to survive in transport to the deep sea. The organic matter moves to the deeper region by the transport of the POM through gravitational flux and to some part also through the active transport of carbon by the vertically migrating zooplankton.

Finally decomposition of the sinking particles, back to nitrate (NO_3^-), carbon dioxide (CO_2) and phosphate (PO_4^{3-}) is achieved by the herbivorous zooplankton consumption and bacterial degradation. This remineralisation increases dissolved inorganic carbon and nutrient concentrations in the deep ocean.

Nutrient remineralisation is the release of organic nutrients to water by organisms to complete the nutrient cycle. Nutrient remineralisation is accompanied by several mechanisms which include the excretion and breaking of cells to release their content. The organic compounds are excreted by producers and processed by heterotrophic organism. Most of the photosynthetic carbon fixation by algae are released into the ocean in a dissolved form which often contains nitrogen and phosphorus. Due to a rapidly circulated virus infection, feeding activities by algevores and many other causes, a large number of the cell to burst and release dissolved organic nutrient into solution.

The limit of carbon removal through the exchange with the atmosphere is by the depth of remineralisation of the exported carbon mixing and upwelling in the ocean causes the carbon dioxide and nutrients to move back to the surface (Sigman & Haug 2003). The rate of primary production in the ocean is maximum in upwelling regions, where remineralised nutrient are brought back from the nutrient-abundant deep waters to the surface (Martin et al. 1987).

1.4 Global meridional overturning circulation

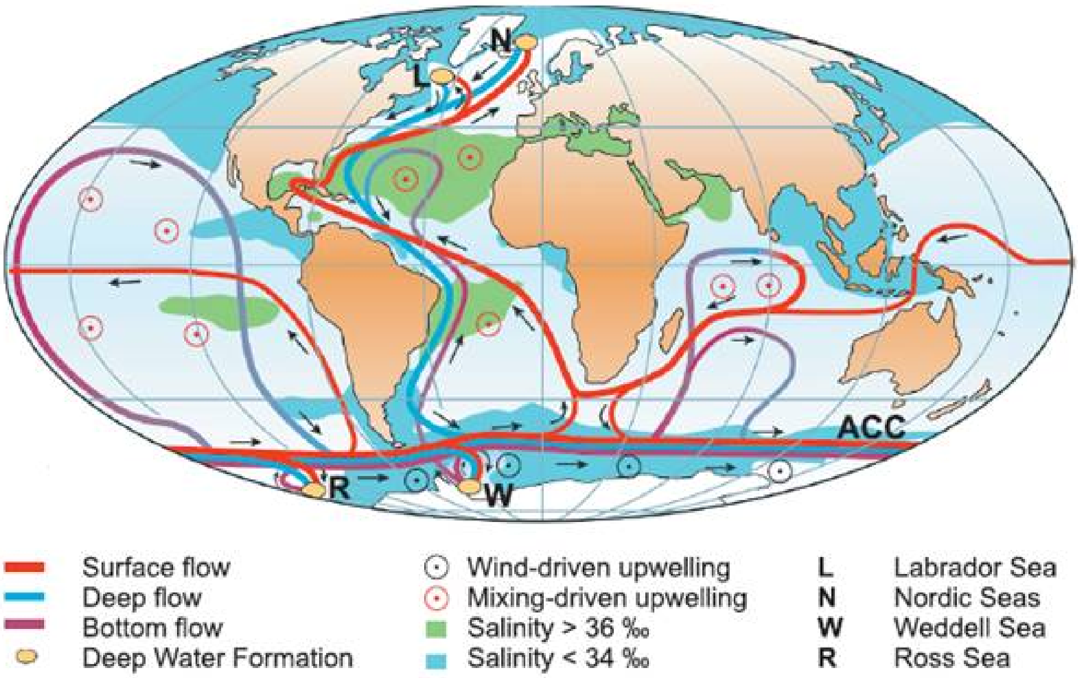

Figure 1.3: *Schematic diagram of the ocean circulation associated with the global Meridional Overturning Circulation (MOC) with special emphasis on the Atlantic branch, AMOC. From (Schmittner et al. 2007).*

The ocean is a continuous motion over many time scales. The major constituents of the large-scale global ocean circulation are the fast upper ocean circulation which is often called the wind-driven circulation, and the slow deep ocean circulation which goes by the name overturning circulation, although in reality the two are interconnected: The deep ocean circulation cells are closed through return currents in the upper ocean which connect the wind-driven ocean gyres at the surface.

The global overturning circulation is a system of surface and deep ocean currents which connects all the basins of the ocean. It has a huge effect on the global climate and support marine life since it is responsible for the redistributing of a large amount of salt, water, heat, oxygen, nutrients, and carbon over the globe and throughout the world's ocean. It connects the surface ocean, which is in direct exchange with the atmosphere, with the deep ocean.

Ocean circulation is driven ultimately by density differences, which is dependent on temperature, salinity, friction of surface winds and modulated by the Coriolis force. Precipitation, evaporation, and sea-ice formation affect the surface salinity of seawater whilst the exchange of heat between the seawater surface and the atmosphere changes the temperature. In a few places, mostly at high latitudes, such as the Labrador Sea or on the shelves of the Antarctic continent, these processes produce surface water masses that are dense enough to sink into depths below a thousand meters or so. This ultimately leads to the formation of two main deep water masses, North Atlantic Deep Water (NADW) and Antarctic Bottom Water (AABW), and where this process occurs is very important to the global ocean circulation. There is a balance between the sinking of the denser water at the polar latitude and upwelling which brings back the water beneath to the surface. Both the formation of AABW and NADW water masses involve surface water and they are regarded in the deep ocean as young age water, i.e. water that has recently been in exchange with the atmosphere. As a results of this, the deep Atlantic Ocean has the highest concentration of oxygen concentration and transient tracers such as chlorofluorocarbons, and the lowest nutrient concentrations since the waters from which NADW formed looses most of their nutrients by biological production during the northward transport of water in the Atlantic.

Most of the North Atlantic Deep Water ultimately comes to the surface in the Southern Ocean, driven by the divergence of Ekman transport caused by the strong winds around Antarctica. Most of the upwelled NADW water moves south and ultimately forms AABW, which spreads into the deep basins of the Atlantic, Indian and Pacific. In the Indian and Pacific, this deep water slowly upwells and mixes with overlying water, to ultimately form the lighter part of the Deep Water that comes again to the surface by upwelling in the Southern Ocean. This water then is advected northward, and subducts again as Subantarctic Mode Water and Antarctic Intermediate Water (AAIW), which then ultimately come to the surface again throughout the subtropics and tropics.

Figure 1.3 describes the ocean circulation connected with the global ocean circulation with special emphasis attached to the flow in the Atlantic ocean, Atlantic Meridional Overturning Circulation (AMOC). AMOC is one of the well-known leading ocean circulation systems and is an essential constituent for the climate system. AMOC is described by a northward flow of warm and salty water in the uppermost layers of the Atlantic as indicated with the red curve, a southward flow of colder water in the deeper Atlantic ocean as indicated with the blue curve in Figure 1.3 and the cooling and freshening of the waters at higher latitudes of the Atlantic around the Labrador and the Nordic Seas. The AMOC is responsible for the transport of a significant amount of heat from the tropics and the Southern hemisphere towards the North Atlantic where heat is released to the atmosphere to influence the climate over large regions. The AMOC has two main overturning primary cells:

1. The upper cell where the northward flow in the upper 1000m ocean waters results in the North Atlantic Deep Water (NADW) which finally returns southward at depths of about 1500m to 4500m.
2. The deep cells where there is a steady rise of water into the lower part of the NADW flowing southward. This is caused by the Antarctic Bottom Water (AABW) that flows northward below a depth of approximately 4500m.

Chapter 2

Physical and biogeochemical model

2.1 Model description

In this study, the Massachusetts Institute of Technology general circulation model (MITgcm), Marshall et al. (1997) is used, coupled with Version 2 of the Regulated Ecosystem Model (REcoM-2). MITgcm constitutes the physical circulation part of the model and REcoM-2 is the ecosystem and the biogeochemical part of the model.

The MITgcm model is a numerical model used to simulate the climate, ocean, atmosphere, or the coupled ocean and atmosphere. It has a single dynamical kernel which allows the simulation of either ocean or atmosphere over a wide range of spatial scales due to the fact that the model can be configured to be non-hydrostatic.

Here a global model configuration without the Arctic Ocean is used on a 2° longitude and 0.38° to 2° latitude i.e 2° (0.38° to 2°) grid. The latitudinal spacing is 2° times the cosine of the latitude in the southern hemisphere for better resolution of the Southern Ocean. To resolve the equatorial undercurrent, the latitudinal resolution is increased to about half of a degree close to the equator (Aumont et al. 1999). The thickness of the 30 vertical layers increases from $10m$ at the surface to $500m$ below the depth of $3700m$ and the model topography is derived from the bathymetry of Timmermann et al. (2010)(Hauck et al. 2013). The model is forced by an annually repeating time series of daily atmospheric fields of wind speed, atmospheric temperature, humidity and shortwave and longwave irradiance taken from the Coordinated Ocean Research Experiments (CORE) reanalysis (Large & Yeager 2009). The model is integrated over 1000 years from a state of rest and from January temperature and salinity fields. The analysed fields are the average over the last 100 model years.

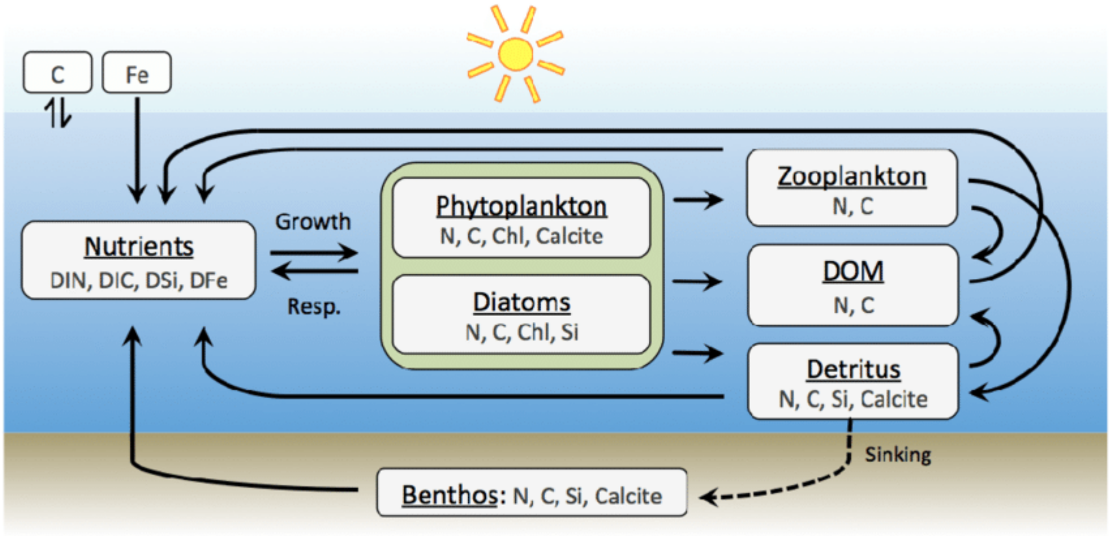

Figure 2.1: *The schematic of the component in the REcoM-2 biogeochemical and ecosystem model by Schourup-Kristensen et al. (2014)*

The REcoM-2 model is the representation of the carbon cycle as well as that of the nutrient elements nitrogen, silicon and iron. It describes the biogeochemistry and a simplified ecology in the ocean with the major organic and inorganic forms of dissolved nitrogen (DIN), silicon (DSi) and iron (DFe), two phytoplankton functional groups (diatoms and nano-phytoplankton), a zooplankton and a detritus compartment (Schourup-Kristensen et al. 2014) as shown in Figure 2.1. The model in total has 21 prognostic tracers, of which eight describe the two main phytoplankton groups. The eight phytoplankton tracers in the model include biomass in units of nitrogen, chlorophyll, silicon, organic carbon and calcium carbonate. The additional tracers are the dissolved nutrients (DIN, DFe, DSi, dissolved inorganic carbon (DIC) and total alkalinity (TA)), detritus with nitrogen, calcium carbonate, biogenic silicate, and dissolved organic nitrogen, organic carbon plus zooplankton biomass in carbon and nitrogen units (Hauck et al. 2013).

The model is based on the Geider et al. (1998) model that allows phytoplankton cells to adopt the internal ratio of their elemental composition to light, nutrient supply, and temperature conditions. Accordingly, the stoichiometric ratio of carbon to chlorophyll (C:Chl) and carbon to nitrogen (C:N) differ in response to different growth conditions.

Detritus sinking speed increases vertically with depth in the ocean and this is parameterized as a linear increase of the sinking speed with depth (Kriest & Oschlies 2011). The REcoM-2 model permits the deposition of sinking material in one single sediment layer, from which it is remineralized and returned as inorganic carbon and nutrients to the lowermost ocean cell.

2.2 The model equations

The biogeochemistry of the ocean in the model is based on mass the balance equation. The rate of concentration change for a tracer is given by the equation:

$$\frac{\partial X}{\partial t} = -(U + \omega) \cdot \nabla X + \nabla \cdot (\kappa \nabla X) + F(X) \tag{2.1}$$

X is the concentration of any biogeochemical variable or tracer and the first two terms on the right-hand side describe the contribution of the physical circulation model which calculates the three-dimensional advection velocity (U), and the diffusivity tensor (κ). ω is the sinking velocity for those tracers that sink, and is constant for diatoms and phytoplankton and linearly increase with depth for detritus. The remaining term $F(X)$ describes the biogeochemical sources and sinks for each individual tracer. It accounts for the biogeochemical processes that increase or decrease the concentration of the tracer. For nutrient tracers, we focus on DIN, DSi and DFe (Hauck et al. 2013).

Nitrite, nitrate and ammonium concentrations together constitute the DIN in the model. DIN taken up by diatoms and nano-phytoplankton constitute the sinks for DIN. The main source of DIN is the remineralisation of dissolved organic nitrogen (DON). DON, in turn, is formed from detrital nitrogen degradation and the discharge of nitrogen by heterotrophs, nano-phytoplankton, and diatoms.
The equation that describes the source and sinks of DIN in the model is:

$$F_{DIN} = -a^N_{phy} \cdot C_{phy} - a^N_{dia} \cdot C_{dia} + \rho_{DON} \cdot f_T \cdot DON \tag{2.2}$$

where a^N_{phy} and a^N_{dia} are the carbon-specific nitrogen assimilation rates for nano-phytoplankton and diatoms respectively, which depend on temperature, photosynthesis rate, and the cellular ratio of nitrogen to carbon N:C (Hauck et al. 2013), (Geider et al. 1998).
C_{phy} and C_{dia} are the carbon biomasses of nano-phytoplankton and diatoms respectively which increase due to the assimilation of carbon in photosynthesis and

decreases the excretion of dissolved organic carbon (DOC), respiration, aggregation, and grazing. $\rho_{DON} \cdot f_T \cdot DON$ is the term that describe the remineralisation of DON to form DIN and f_T is an Arrhenius function of the local temperature.

The transfer from dissolved silicic acid (DSi) to and from biogenic silica in diatoms and detritus constitutes the silicon cycle in the model. The silicate sink in the water column by silicate assimilation, whilst the degradation of detritus silica contributes to the source of DSi in the model.
The equation that describes the sources and sinks of the DSi in the model is therefore given by:

$$F_{DSi} = -a^{Si}_{dia} \cdot C_{dia} + \rho^{T}_{Si} \cdot Si_{det} \tag{2.3}$$

Where a^{Si}_{dia} is the carbon-specific silicate assimilation rate diatoms which depend on the Arrhenius function of the local temperature and the N:C and Si:C uptake ratio. C_{dia} is the carbon biomass of detritus, ρ^{T}_{Si} is the temperature dependent silicate dissolution rate. Si_{det} is the biogenic silica in detritus formed from grazing, excretion and aggregation of diatoms.

Dissolved iron (DFe) in the model is the sum of the free or inorganically bound iron concentration Fe' and organically complexed iron bound to a ligand Fe_L. The organic and inorganic forms are assumed to be in equilibrium and calculated at each time step by applying the law of mass action for the reaction: $Fe_L = Fe' + L'$. With L' representing the free ligands and a prescribed total ligand concentration. Iron is cycled in the model proportional to nitrogen, with a fixed Fe:N ratio. In addition, iron is lost to particles by adsorption or 'scavenging' and is brought into the ocean by deposition of dust and by release from the sediment. Scavenging is proportional to the detritus carbon used to represent the mass of sinking particles. Respiration of phytoplankton and heterotrophs, remineralization of DON and excretion of heterotrophs are the biogenic sources of dissolved iron in the model. The sources and sinks of DFe in the model are written mathematically as:

$$\begin{aligned} F_{DFe} = q^{Fe} \cdot ((\epsilon^{N}_{phy} - a^{N}_{phy}) \cdot C_{phy} + (\epsilon^{N}_{dia} - a^{N}_{dia}) \cdot C_{dia} + (\epsilon^{N}_{het}) \cdot C_{het} \\ + \rho_{DON} \cdot f_T \cdot DON) - \kappa^{scav}_{Fe} \cdot C_{det} \cdot Fe' \end{aligned} \tag{2.4}$$

Where q^{Fe} is the iron to nitrogen ratio (Fe:N) which is assumed to be constant for all processes. Through this assumption, iron concentration and carbon concentration are connected. ϵ^{N}_{phy}, ϵ^{N}_{dia} and ϵ^{N}_{het} is the nitrogen excretion rate for nanophytoplankton, diatom and heterotrophs. κ^{scav}_{Fe} is the iron scavenging rate.

It depends on the rates of nutrient assimilation. C_{phy}, C_{dia}, C_{het} and C_{det} are the carbon biomass of nanophytoplankton, diatom, heterotrophs and detritus respectively. a^N_{dia} and a^N_{phy} are the nitrogen-specific silicate assimilation rate diatoms and nanophytoplankton respectively.

2.3 Data for initialisation and comparison

The model was initialised with temperature, salinity, oxygen, nitrogen and silicon fields from the World Ocean Atlas 2009, WOA09 (Johnson 2010), (Garcia et al. 2010), (Locarnini et al. 2010). This dataset is made up of the information on monthly, annual and seasonal climatology and statistical distribution of the fields. This is obtained by analysing observed profiles in a regular global grid at a one-degree latitude-longitude resolution and at selected standard depths on a 33 uneven spaced depth levels from the surface to a maximum depth of $5500m$. Based on the ocean bottom depth and land, a quarter-degree land mask was created from the ETOPO5 topography/ bathymetry dataset land mask (Amante & Eakins 2009). For comparison of the WOA09 data with the model, the WOA09 was interpolated both vertically and horizontally to the model grid.

2.4 Methods for model-data comparison

A quantification of the comparison between model and the climatological data can be done in a number of ways. Among those, the root-mean-square deviation (RMSD), the bias and the correlation coefficient are most often used.
In order to measure how far, on average, the model and data are apart, the RMSD is used. It is the average distance between the modelled and the observed variables and disregards whether the deviations are positive or negative. It has the same unit as the observational data.
The RMSD can be calculated mathematically by:

$$RMSD = \sqrt{\frac{1}{n}\sum_{i=1}^{n}(P_i - O_i)^2} \tag{2.5}$$

where O_i and P_i are the observations and model predictions respectively, n is the number of data points and i is the index that enumerates the observations.

The difference between the averages of the observations and the averages of the modelled predicted values gives the average absolute error (bias). A bias near zero can mislead since the positive and negative differences can cancel each other. The bias can be calculated from the equation

$$Bias = \frac{\sum_{i=1}^{n}(P_i - O_i)}{n} = \bar{P} - \bar{O} \tag{2.6}$$

where and $\bar{O}$ and $\bar{P}$ are respectively the observation and prediction averages.

The correlation coefficient (sometimes also called the Pearson correlation coefficient) measures the linear correlation between the model and the actual data, i.e. the tendency of covariation between the model and the predicted data. It ranges from -1 to 1, with positive values representing the linear proportional variation of the model and predicted data. $+1$, -1 and 0 represent respectively a strong positive, negative and no relationship. The correlation coefficient, r can be calculated mathematically by:

$$r = \frac{\sum_{i=1}^{n}(O_i - \bar{O})(P_i - \bar{P})}{\sqrt{\sum_{i=1}^{n}(O_i - \bar{O})^2 \cdot \sum_{i=1}^{n}(P_i - \bar{P})^2}} \tag{2.7}$$

To compare modelled and observed concentrations with the methods mentioned above, it is required that the model and the data are corresponding. In this case, the WOA09 and the model were defined on different grid points. One additional step is, therefore, to interpolate the data grid first to the model grid points using linear interpolation in Matlab.

Both data and observations are defined on a latitude-longitude grid and on an unevenly spaced vertical interval. One grid box, therefore, can have different volumes with boxes in higher latitudes and near the surface typically representing less volume than those in low latitudes. This problem is rectified using weighted averages with the grid-box volume as a weight to calculate the means in equations 2.5 to 2.7.

2.5 Model experiments

In accessing the role of overturning on nutrient and oxygen distribution in the global ocean, several tuning experiments were carried out in addition to a standard model set-up for the physical and biogeochemical processes. The changes in two experiments were increased ($800m^2s^{-1}$)and decreased ($400m^2s^{-1}$) values of the diffusivity constant in the Gent-McWilliams parameterization which describes the effect of non-resolved eddies in a coarse resolution model (Gent et al. 1995) from the standard ($600m^2s^{-1}$). A third experiment modifies the topography in the Denmark Strait (Figure 2.2) from the original Timmermann et al. (2010) bathymetry that was specified in the RECoM model configuration. The modification was done to make the Denmark Strait shallower. This is a key region for the formation of several water masses like the North Atlantic Deep Water, NADW since it determines the strength of the overflow from the Greenland Sea into the North Atlantic. Other models have used subjective changes in the topography to get a reasonable overturning through this passage by widening or changing the sill depth width (Willebrand et al. 2001).
Modifying the Denmark Strait was important because, together with the Faroe Bank channel are the pathway for dense water from the Arctic Nordic sea into the North Atlantic and plays a major role in the strength of the overturning circulation (Lohmann 1998).

Other experiments were conducted to increase the remineralisation depth of the nutrient tracers. The distribution of nutrients in the ocean is affected by two factors, the sinking speed of particles and the remineralisation rate. The sinking speed of detritus in the model increases linearly with depth (Kriest & Oschlies 2008). This can be written mathematically as:

$$Sinkingspeed, w_{det} = w_0 + A \cdot Z \tag{2.8}$$

where w_0 is the sinking speed at the surface and Z is depth and A is the vertical gradient of the sinking speed. In all the model runs, the surface sinking speed is set to 20 $mday^{-1}$ and the initial value of A set to 0.0288 day^{-1}. This means at 1000 m depth, the sinking speed is: $w_{det} = 20 + 0.0288 \cdot 1000 = 48.8mday^{-1}$.

$$Sinkingspeed, w_{det} = 20 + 0.0288 \cdot 1000 = 48.8mday^{-1} \tag{2.9}$$

In two of the models run the factor A was increased by 11.11% ($0.036day^{-1}$) and 50% ($0.0432day^{-1}$).

The remineralisation of detritus was also modified in two of the model runs. The detritus remineralisation is proportional to the detrital concentration multiplied by the remineralisation rate constant, which differs for detritus nitrogen and carbon. In the standard model the remineralisation rate for nitrogen and carbon is set to $0.165 day^{-1}$ and in the sensitivity model runs, the remineralisation rate of nitrogen and carbon was reduced by 13.3% ($0.143 day^{-1}$) and 26.6% ($0.121 day^{-1}$). Both reductions have effect that the detritus remineralisation is shifted downward with particles sinking deeper before being remineralised. The simulations made are summerised in the Table 2.1 below.

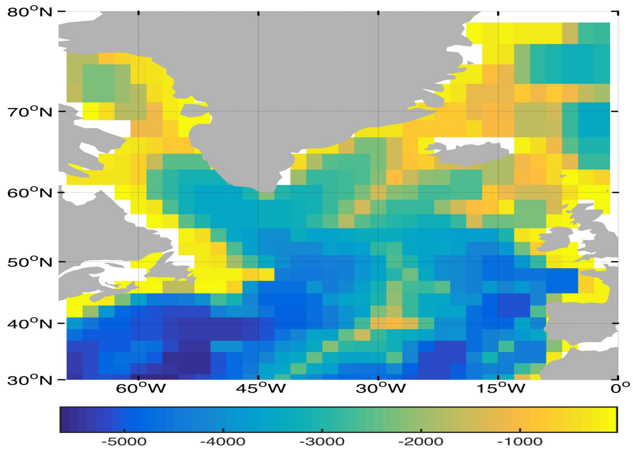

Figure 2.2: *Standard bathymetry at the Denmark Strait*

Table 2.1: Summary of different model simulations.

Name	Model Description
Run 1	Standard Model run
Run 2	Model with decreased GM diffusivity constant ($400 m^2 s^{-1}$)
Run 3	Model with increased GM diffusivity constant ($800 m^2 s^{-1}$)
Run 4	Model run with modified Denmark strait topography
Run 6	Model run with 11.11% increase in sinking speed factor
Run 7	Model run with 13.3% remineralisation constant reduction
Run 8	Model run with 50% increase in sinking speed factor
Run 9	Model run with 26.6% remineralisation constant reduction

Chapter 3

Results from the standard model run

3.1 Physical model

Describing the physical properties of the ocean starts with a description of their spatial variations. Properties such as temperature, salinity, oxygen concentration and nutrients are set by exchanges at the ocean surface and, in the case of nutrients and oxygen, change in the interior of the ocean by the formation and remineralisation of organic matter. Their distributions can, therefore, be used to define the vertical and horizontal flow of water from sinking, upwelling, mixing and precipitation by assuming that the properties of seawater at the surface are similar within a given region. This chapter reviews how the main oceanic water masses are represented in the zonally averaged temperatures and salinity fields from WOA09 data and the MITgcm model output.

3.1.1 Atlantic zonally averaged salinity

The zonally averaged Atlantic salinity for the standard model run is shown in Figure 3.1 together with the interpolated observational data from WOA09 and the model-data differences.

The model zonally averaged salinity in the Atlantic ocean is shown in Figure 3.1a. The salinity is about 36 to 37.5 near the surface in the tropics and subtropics. These maximum values at the surface of the subtropics in the Atlantic are driven by high evaporation exceeding precipitation. The contribution of this saline water to the formation of NADW makes NADW also comparatively saline. The AAIW has the lowest salinity in the Atlantic between about 33.4 to 34.2. The northward flow of AABW, which spreads from the Southern Ocean into the deep Atlantic

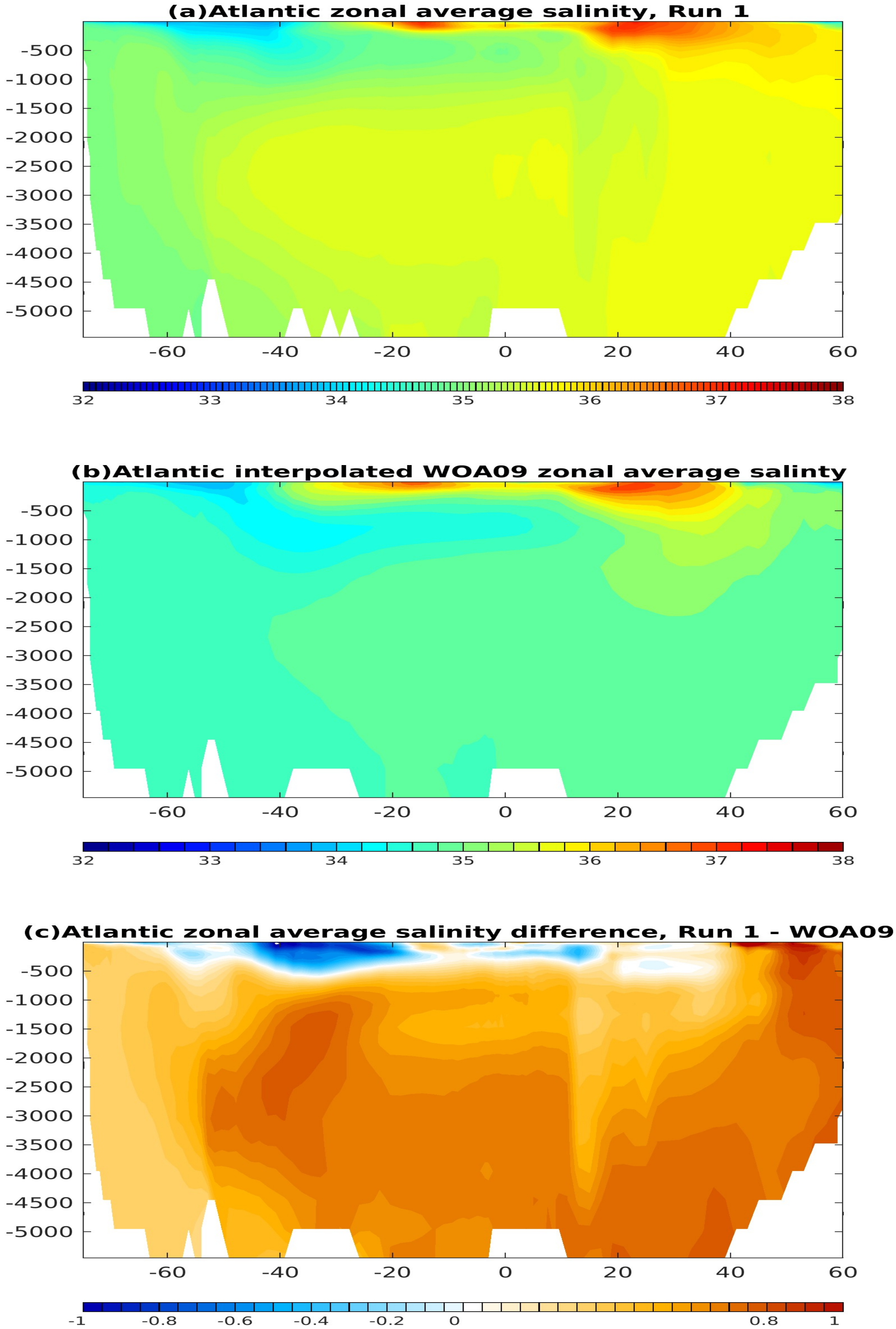

Figure 3.1: *Zonally averaged Atlantic salinity right for model(a), interploated WOA09(b) and the differences in salinity(c)*

Ocean, has higher salinity (34.8 to 35.2) compared to the AAIW. The northern sourced NADW at depths between 500m and 5000m has moderately large values of salinity between 35.3 to 36.0 compared with those of the AABW and AAIW.

For the observational zonal averaged salinity as shown in the middle of Figure 3.1, the salinity pattern is qualitatively similar to that of the model at the surface of the tropics and the subtropics where a maximum salinity of about 36.8 is recorded. The AAIW has a minimum salinity of about 33.9 and increases to about 34.9 beneath the South Atlantic subtropics to the equator between 200m and 1500m. The northward flowing southern sourced AABW is also a little bit saltier, with a salinity approximately 35.1. The northward sourced NADW is also relatively saltier (between 35.3 and 35.7) than the AABW.

The difference in the pattern between the model and the observational data is shown in Figure 3.1c. At the northern and lower latitudes of the Atlantic ocean, there is a negative difference with salinity differences between -1 and -0.3. One reason is that the fresh AAIW is shallower (up to between 1000m depth) in the model than the observations. A further reason is a missing inflow of the Mediterranean outflow water in the model, which leads to an underestimation of salinity in the region. The negative values reflect a weak, shallow AAIW in the observational data from the WOA09. All the water masses that are below the AAIW have positive differences between 0.3 and 1. This means the model NADW and AABW have a higher salinity than the observations since the figure shows positive anomaly. The Southern Ocean also has relatively high positive anomaly.

3.1.2 Atlantic zonally averaged temperature

For the zonally averaged temperature for the model run (Figure 3.2a), the annual average mixed layer temperature in the tropics and the subtropics is high due to high solar irradiance. Below this warm water which extends deeper in the subtropics than near the equator indicating upwelling at the equator and downwelling in the subtropics, one finds the AAIW in the southern hemisphere which extends between about 500m and 1000m depths. There is also a huge region of southward-flowing NADW which extends up to about 40°S from 60°N. Below the NADW a northward flow of very cold water can be seen which is the AABW. This water mass shows temperature increases as the water moves northward. The Southern Ocean is very cold i the Atlantic.

Figure 3.2b shows the zonally averaged temperature for the observational data. It shows a quantitatively similar pattern to the model run. The maximum temperature values can be found in the tropics and the subtropics. There is also AAIW which is characterised by low temperatures in the South Atlantic. The

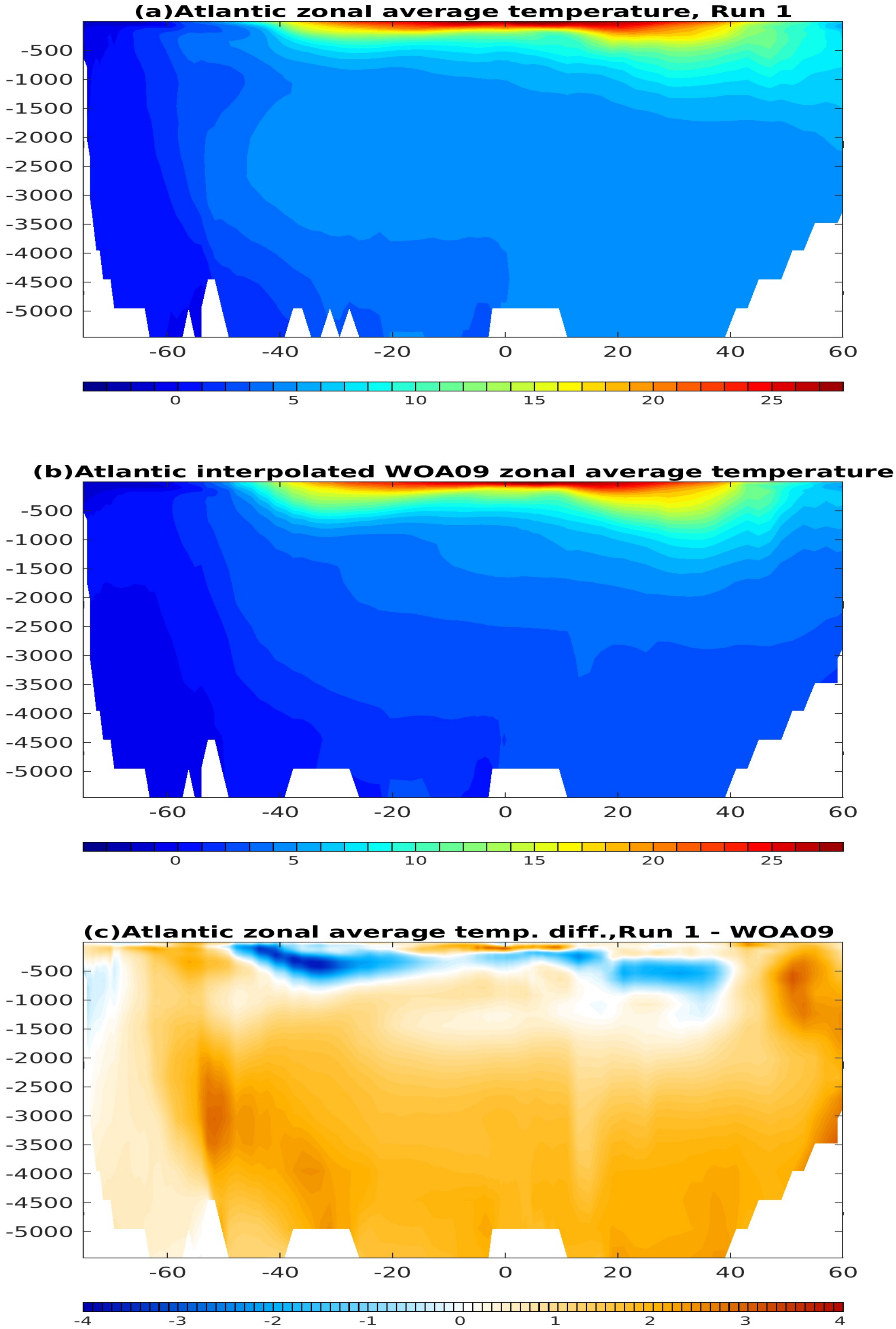

Figure 3.2: *Zonally averaged Atlantic temperature for model(a), interploated WOA09(b) and the differences in temperature(c) (°C)*

NADW is also well represented, but its temperature decreases with depth to the floor. The extremely cold southern sourced AABW has the minimum temperature in the Atlantic Ocean according to the observational data. The 2°C to 4°C isotherm patterns of the model extends deeper than in the observational data. The Southern Ocean is also very cold in the Pacific.

The differences in the Atlantic zonally averaged temperature between the model and the observational data are shown in the lower figure. At lower latitudes surface thermocline in the tropics and subtropics, the model is warmer than the observational data at the surface to about 1000m and vice versa at higher latitudes. The southern sourced water mass of the AABW and the Southern Ocean is the coldest in both the model and the observational data. It can be observed that there is a large negative temperature difference mainly in the low latitude subsurface thermocline in the tropics and subtropics. The difference is about -1.7°C to -3°C, which means the model is quite colder than the WOA09 observational data. This is because the AAIW, which is colder than the water above it, is shallow and a little bit too far north in the model. The deep Atlantic Ocean and high latitudes have a high-temperature difference, meaning the model at these regions is warmer than the observations between 1.3°C to 2.9°C.

3.1.3 Pacific zonally averaged salinity

The Pacific zonally averaged temperature and salinity for the model, the corresponding observational data from the WOA09 and the model-data differences are shown in Figure 3.3.

The salinity in the Pacific for the model, shown in Figure 3.3a, shows the highest salinity in the subtropical Pacific of about 35.5. The North Pacific Intermediate Water, NPIW is the least saline in the Pacific with a salinity of roughly 33.5 to 34.2. The shallow South Pacific Intermediate Water, SPIW has relatively low salinity between 34.2 to 34.5. Both the intermediate waters in the model extend up to about 1000m depth. There is also the saltier Southern Ocean and the Pacific Bottom water, PBW which flows northward and fills the deep Pacific with the salinity of about 34.9 to 35.2.

The observational data also shows the highest salinity at the surface of the tropics and subtropics in the Pacific as shown in Figure 3.3b. The SPIW has low salinity between 34 to 34.5 and the lowest value is found in the NPIW of approximately 33.5 to 34.2. But the two water masses extend up to about 1700m depth. The southern sourced PBW and the Southern Ocean are relatively saltier compared with that at the surface of the subtropics with values between approximately 34.6 to 34.8. There is also relatively low salinity NADW which flows southward.

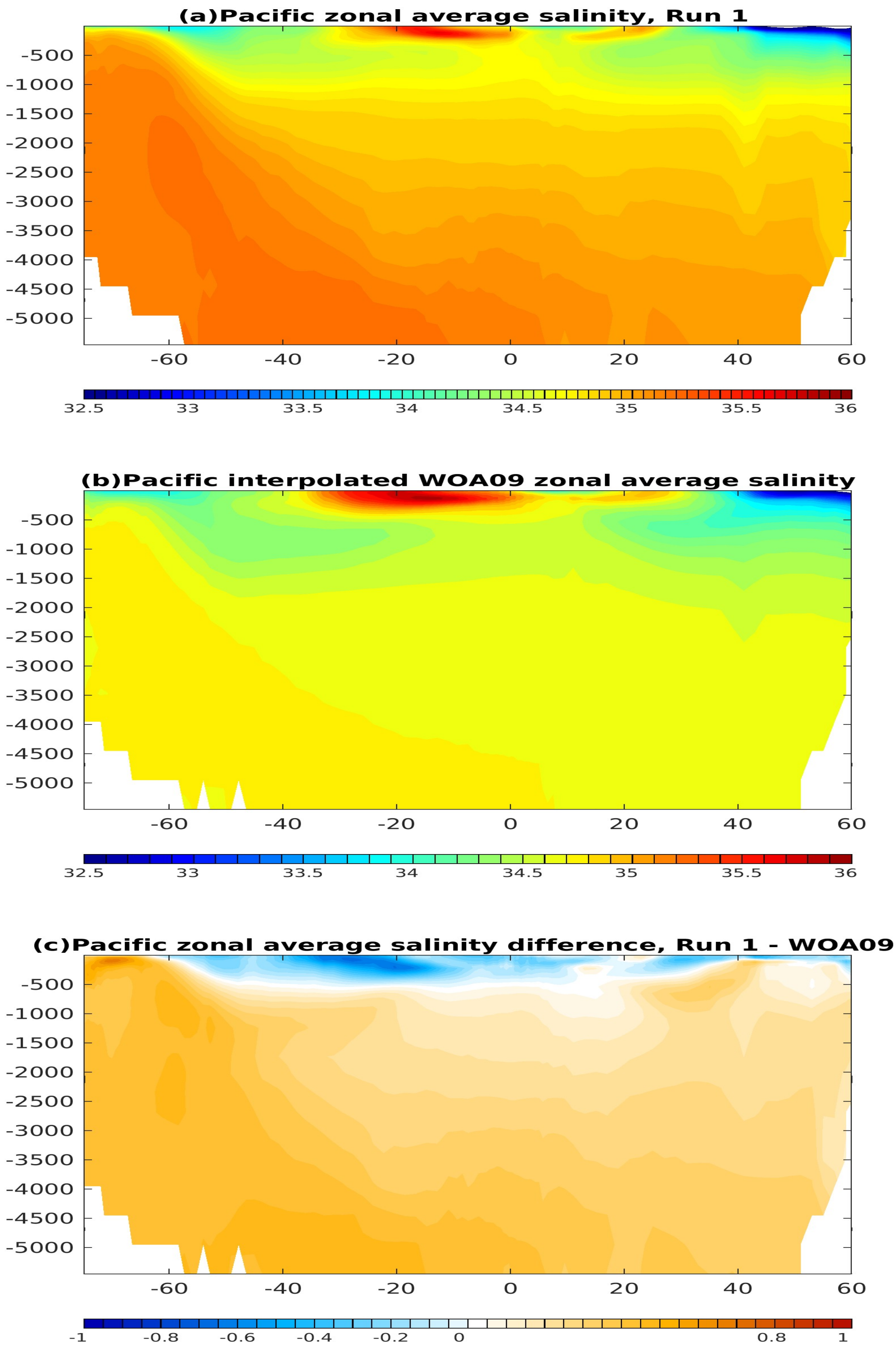

Figure 3.3: *Zonal averaged Pacific salinity for model(a), interpolated WOA09(b) and the differences in salinity(c)*

From the difference between the model and the observation data in the Pacific zonal salinity plot in Figure 3.3c, there is a negative anomaly in the upper $500m$

in the surface thermocline low latitudes of the Pacific. This may be because both intermediate waters are shallower in the model compared to the observation. The rest of the Pacific is saltier in the model than in the observation. This is true for the Southern Ocean,NAPW and the PBW.

3.1.4 Pacific zonally averaged temperature

The surface of the tropics and subtropics in the Pacific are warm for the model just like in the Atlantic Ocean which can be seen in Figure 3.4 (upper), which extends up to about 1200m depth. The deeper Pacific is colder than the deep Atlantic ocean. Unlike the North Atlantic, the North Pacific has no deep water formation. The Southern Ocean northward flowing PBW fills a large region of water in the Pacific Ocean have the lowest temperature ranges in the Pacific. The South Pacific Intermediate Water, SPIW fills a very small area in the South Pacific.

The observational data also has no NPDW but NPIW which is very cold, weak, shallow and covers a very small region. The surface temperature from the middle figure of Figure 3.4, shows high values at the surface and subsurface thermocline in the tropics and subtropics extending up to about 500m. The SPIW covers a small region of water in the North Pacific with temperatures. The northward flow southern sourced PBW covers a large region of the ocean and has temperature range which decreases with depth. The Southern Ocean is the coldest compared with the rest of the water masses.

For the model-observational data difference of zonal average temperatures differences in the bottom figure, there are high positive values at the surface signifying higher model surface temperature with values approximately 3.2°C to 3.6°C. The positive difference in the southern ocean and deep Pacific signifies comparatively high mean PBW temperature in the model. Both intermediate water masses are weaker and too shallow in the model North Pacific. The mid-latitude Pacific, from about 800m to 3000m between 55°S and 60°N, has negative values meaning the observed temperature is higher than in the model. This may be an indication that the formation of the PDW is too strong and pushes the intermediate waters upward or that the vertical diffusion of heat is too weak.

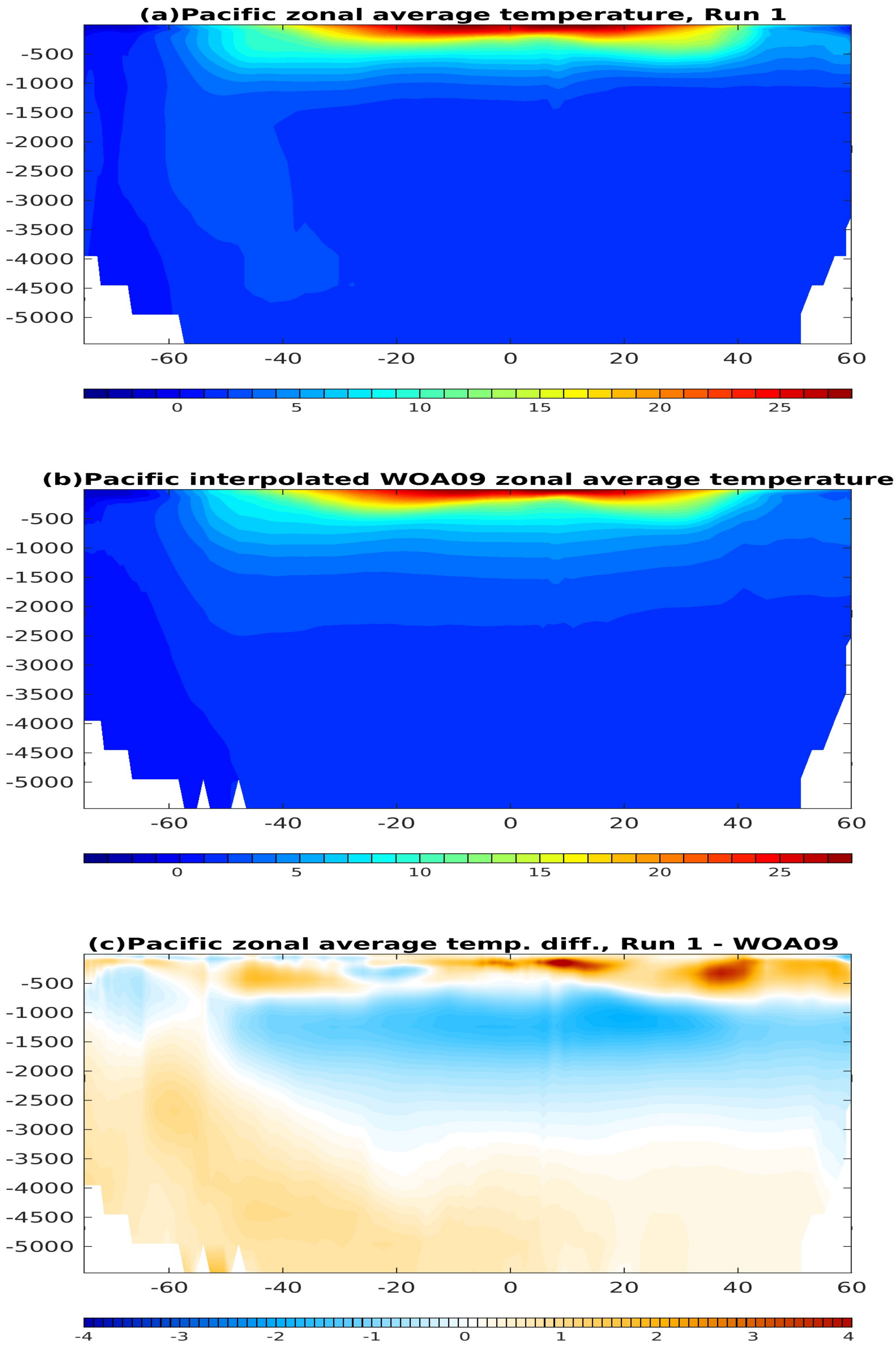

Figure 3.4: *Zonal averaged Pacific temperature for model(a), interpolated WOA09(b) and the differences in temperature(c) (°C)*

3.1.5 Atlantic meridional overturning circulation

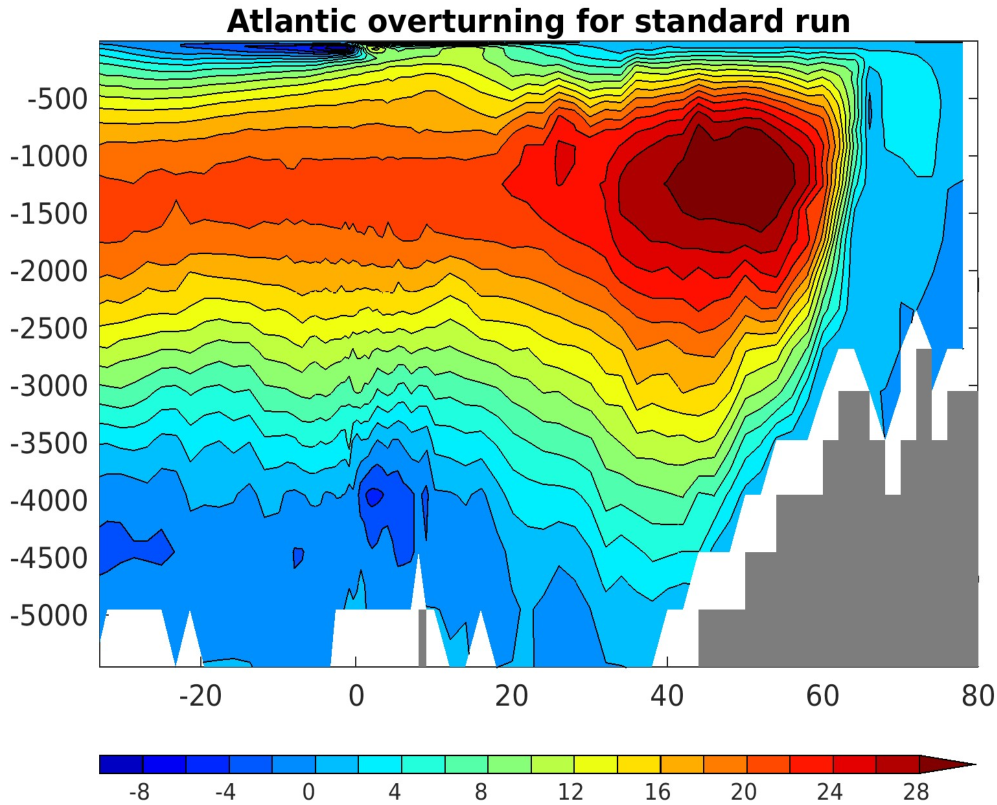

Figure 3.5: *The Atlantic meridional overturning circulation by the REcoM-2 standard model run(Sv)*

The transport and the large scale circulation in the ocean are described by several means of which the horizontal barotropic stream function and the meridional overturning circulation are the most important ones. The Atlantic meridional overturning circulation, AMOC is crucial in the transport of a significant amount of heat from the tropics and the southern hemisphere towards the North Atlantic where heat is released to the atmosphere to influence the climate over large regions (Jungclaus et al. 2013).

Figure 3.5 shows the Atlantic meridional overturning circulation for the RECoM-2 model which is characterized by the overturning stream function which can be written as:

$$\psi(y,z) \quad = \quad \int_0^z \int_{x_1}^{x_2} V(x',y,z')dx'dz' \tag{3.1}$$

where V is the annually averaged meridional or northward velocity, y and z is the latitude and depth respectively, x_1 is the longitude of the coast of America and x_2 is the longitude of the coast of Africa and Europe.

In the model, the general characteristics of AMOC is shown in Figure 3.5. It is characterised by an upper and a lower cell. The upper cell describes the northward flow of warm and salty water in the uppermost layers of the Atlantic and a southward flow of cold and relatively low saline water in the deeper Atlantic ocean which has freshened and cooled at the surface in the North Atlantic subpolar. The lower cell is driven by the inflow of the AABW which mixes with the lower part of the NADW and return southward.

In the upper cell, there is a clockwise overturning circulation with the dense North Atlantic Deepwater NADW formation which flows northward at the surface and the southward return flow of the NADW to the surface. Mixing and buoyancy loss in the North Atlantic increases the density of the surface water which then sinks to the deep ocean. Below the clockwise NADW is the anticlockwise cell representing the inflow of the dense Atlantic Bottom Water, AABW which is formed on the Antartic shelves around the Antartica and then flows northward which then returns southward with the NADW and reappear again around Antarctica. The upper cell is pretty strong and northward transport of the AABW across the 24°N is 23.3Sv compared with the 18.0 $\pm$ 2.5 Sv as estimated in Lumpkin & Speer (2007). The lower cell as shown is relatively weak. The magnitude of the northward flow of the AABW across the 26.5°N is -1.2Sv compared with the observational RAPID data from Kanzow et al. (2010) is around -2Sv. The MPI-ESM-MR and the MPI-ESM-LR simulations had around -3.4Sv and -2.8Sv respectively in Jungclaus et al. (2013). The maximum overturning is 31Sv at 52°N compared with the 17Sv from Stouffer et al. (2006) and 19Sv in the Rennermalm et al. (2007) UVic ESCM model estimations. From the figure, the zero contour depth, which is the depth at which the upper NADW is separated from the lower AABW, is between 3500m and 3700m which conforms to the 3500m to 4000m boundary between the upper and lower cell in the RAPID data from Kanzow et al. (2010). Most models of comparative resolution produce a much shallower NADW in contrast to observations (e.g. Jungclaus et al. (2013)).

3.1.6 Barotropic streamfunction

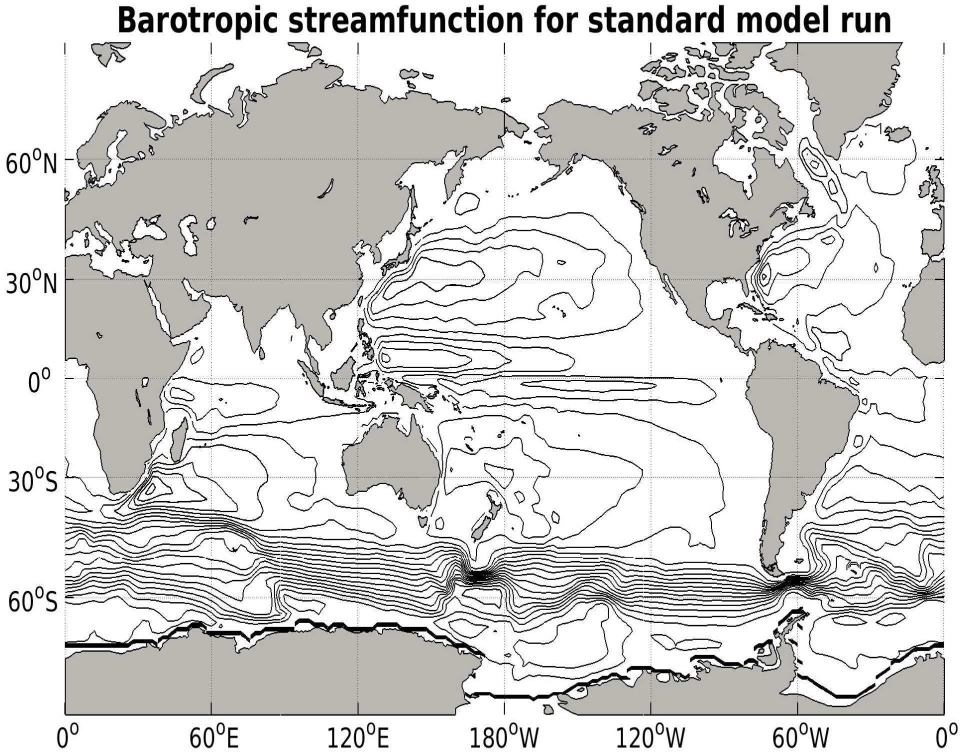

Figure 3.6: *Barotropic streamfunction, standard model run(Sv)*

The barotropic streamfunction represents the integral of the horizontal velocities from the ocean surface to the abyss. It can be mathematically written as:

$$\psi_{Barotropic}(x, y) = \int_{y0}^{y} \int_{0}^{H} U(x, y', z') dz' dy' \tag{3.2}$$

where U is the annually averaged zonal (westward) velocity, y_o is a reference point on a coast, where the streamfunction is zero, e.g the coast of Antarctica.

Figure 3.6 reproduces some of the familiar characteristics of the ocean gyres and the large current systems. The subtropical gyre in the North Atlantic has a maximum transport at the Gulf Stream and extends to Europe and the western part of North Africa with about $34Sv$. This is compared with the $28Sv$ from the Max-Planck Institutes-Earth system Model-Low Resolution, MPI-ESM-LR and the $37Sv$ in the MPI-ESM-Mixed Resolution, MR model in Jungclaus et al. (2013) and $34Sv$ observational estimate transport from Clarke (1984). The subtropical gyre associated with the Kuroshio in the North Pacific Ocean has a maximum transport of about $86Sv$ and extends towards the Oyashio in Southern Japan compared with the estimated transport values of $80Sv$ for MPI-ESM-LR and $60Sv$ for MPI-ESM-MR model estimates from Jungclaus et al. (2013) and $42Sv$ Imawaki et al. (2001).

The Antarctic Circumpolar Current, ACC is the strongest global current around Antarctica. The transport between South America and Antarctica is approximately $133Sv$ which is very close to the measurements made by different methods such as the 136.7 ± 7.8 Sv from Cunningham et al. (2003), $134 \pm 14Sv$ by Nowlin Jr & Klinck (1986) and $134 \pm 13Sv$ from Whitworth III & Peterson (1985), $140Sv$ by Ganachaud & Wunsch (2000) but disagrees with the $175Sv$ extimated by Colin de Verdière & Ollitrault (2016).

3.2 Biogeochemical model

3.2.1 Zonally averaged nitrate and oxygen

The distribution of nitrate globally shows some common major characteristics. Surface and the thermocline waters in the subtropical and tropical ocean are low nitrate waters which extends to about $300m$. Then there is a broad maximum which keeps apart and being at the center of the equator 15°S and 15°N. This maximum can be seen between $500m$ to $1000m$ in the equatorial region. Nutrients at the Southern Ocean is relatively high all through the water column. The distribution of DIN and oxygen in the Atlantic and the Pacific Oceans are shown in Figure 3.7 through to Figure 3.10.

3.2.2 Atlantic zonally averaged nitrate

The distribution of nitrate in the Atlantic Ocean as shown in Figure 3.7 conforms to the flow of major water masses. For the standard model ocean DIN distribution shown in Figure 3.7(upper), the surface water is depleted in DIN. The subsurface thermocline in the tropics and subtropics are very rich in nitrate and which has the maximum nitrate concentration in the Atlantic extending between $300m$ to $1300m$ and 30°S to 20°N across the equator. The AAIW is also nitrate but the concentration decreases as the water mass flows northward. At the high of the southern Atlantic, between 70°S - 50°S, the AABW has high uniformly distributed DIN concentration. The northern sourced NADW is also DIN depleted and slightly increases as the water mass flows southward.

The interpolated WOA09 also has the surface of the tropics and subtropics low latitudes depleted with nitrate which is the lowest in the Atlantic Ocean as can be seen in Figure 3.7(middle). The subsurface thermocline nitrate concentration

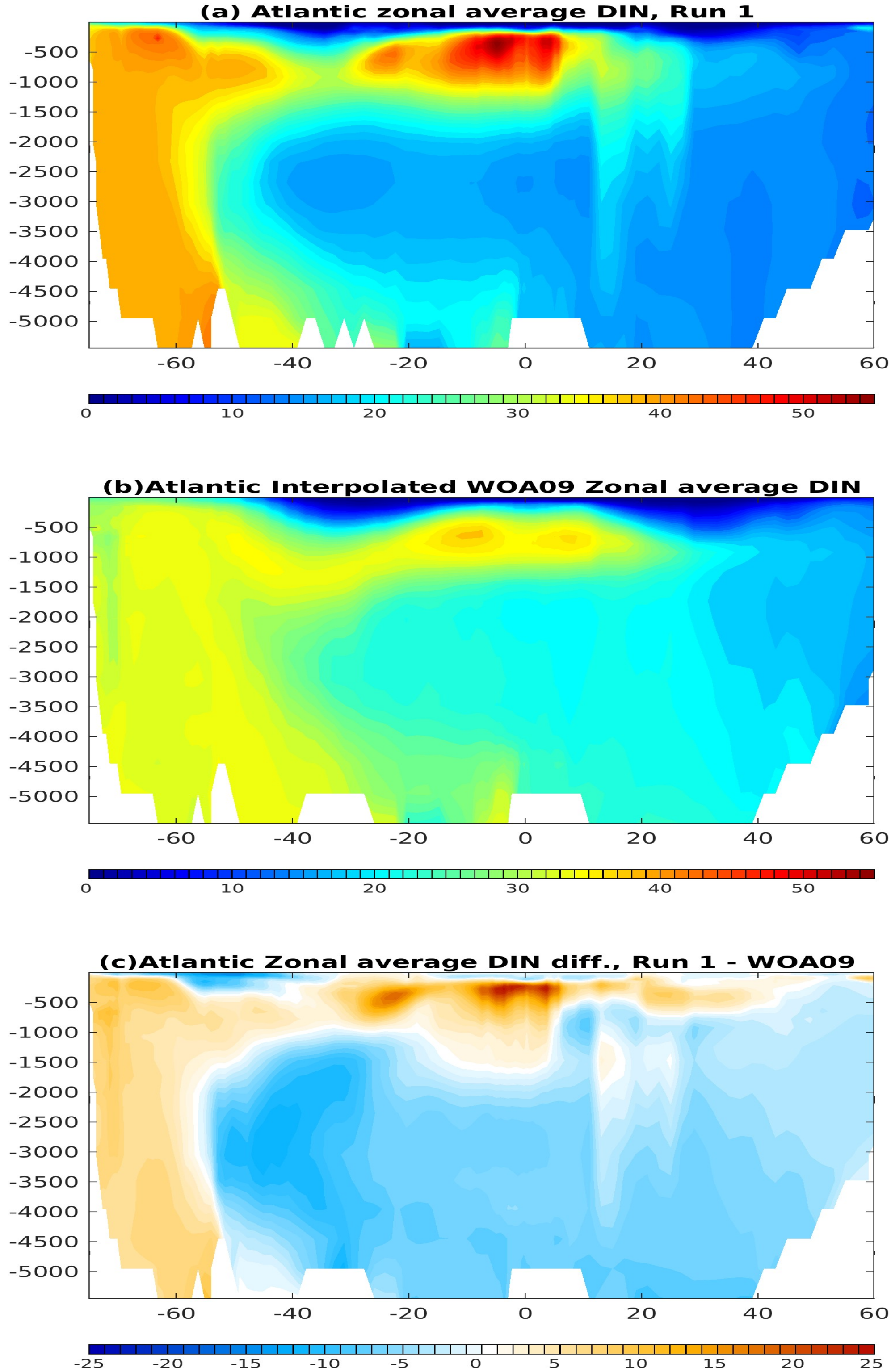

Figure 3.7: *Zonally averaged Atlantic DIN for model(a), interpolated WOA09(b) and their differences(c)* ($\mu molL^{-1}$)

in the tropics and subtropics, AAIW, AABW and the entire Southern Ocean are nitrate-rich. There is maximum at the equatorial thermocline tropics and subtropics since there is always high biomass production which leads to low nutrients at the surface and remineralisation of the water column at the subsurface of the equator. In the NADW the water mass is strongly remineralised which is not the case for the model (slightly remineralized).

For the model - observational data zonal average DIN in the Atlantic ocean as shown in the bottom figure of Figure 3.8. The surface thermocline in the tropics and subtropics, AAIW, AABW and the entire Southern Ocean has a positive nitrate difference which is consistent with the explanation that remineralisation occurs at the subsurface of the Atlantic Ocean in the model more than in the observational data. This makes the nitrate concentration higher in the model than the observation. The northern sourced NADW has negative DIN anomaly which decreases further as the water mass moves from north to the south extending up to about 50°S indicating the interpolated observational data has high nitrate concentration since the remineralised nitrate sinks into the deeper ocean in the WOA09.

3.2.3 Atlantic zonally averaged oxygen

The zonally averaged dissolved oxygen over the Atlantic Ocean is shown in Figure 3.8. The upper figure shows the modelled dissolved oxygen has oxygen-rich AAIW which is very concentrated in its formation but decreases strongly along its path. The thermocline in the tropics and subtropics, AABW and the entire Southern Ocean has minimum oxygen concentration with the lowest at the mid-depth equatorial tropics and subtropics. One possible reason is the fact that there is more warming at the equatorial surface water and respiration of sinking organic matter. The southward flow NADW as well as the surface waters of the North and South Atlantic high latitude is also oxygen-rich. The NADW decreases the oxygen concentration as it moves southward to the southern ocean.

The interpolated WOA09 zonal averaged oxygen shows some similar characteristics to the model as can be seen in the middle figure. The north and south high latitude surface waters is shown to have high oxygen concentration. The surface and subsurface thermocline in the equatorial tropics and subtropics are depleted in oxygen.The AAIW has the highest oxygen concentration but decreases along its path. This can be attributed to the very cold and fresh AAIW for the observational data as shown in the middle figures of Figure 3.1 and 3.2. The AABW and the Southern Ocean has a little bit less oxygen concentration but increases along its path to the bottom. This may be attributed to the fact that the observational AABW gets colder with depth as can be seen in Figure 3.1b.The NADW has

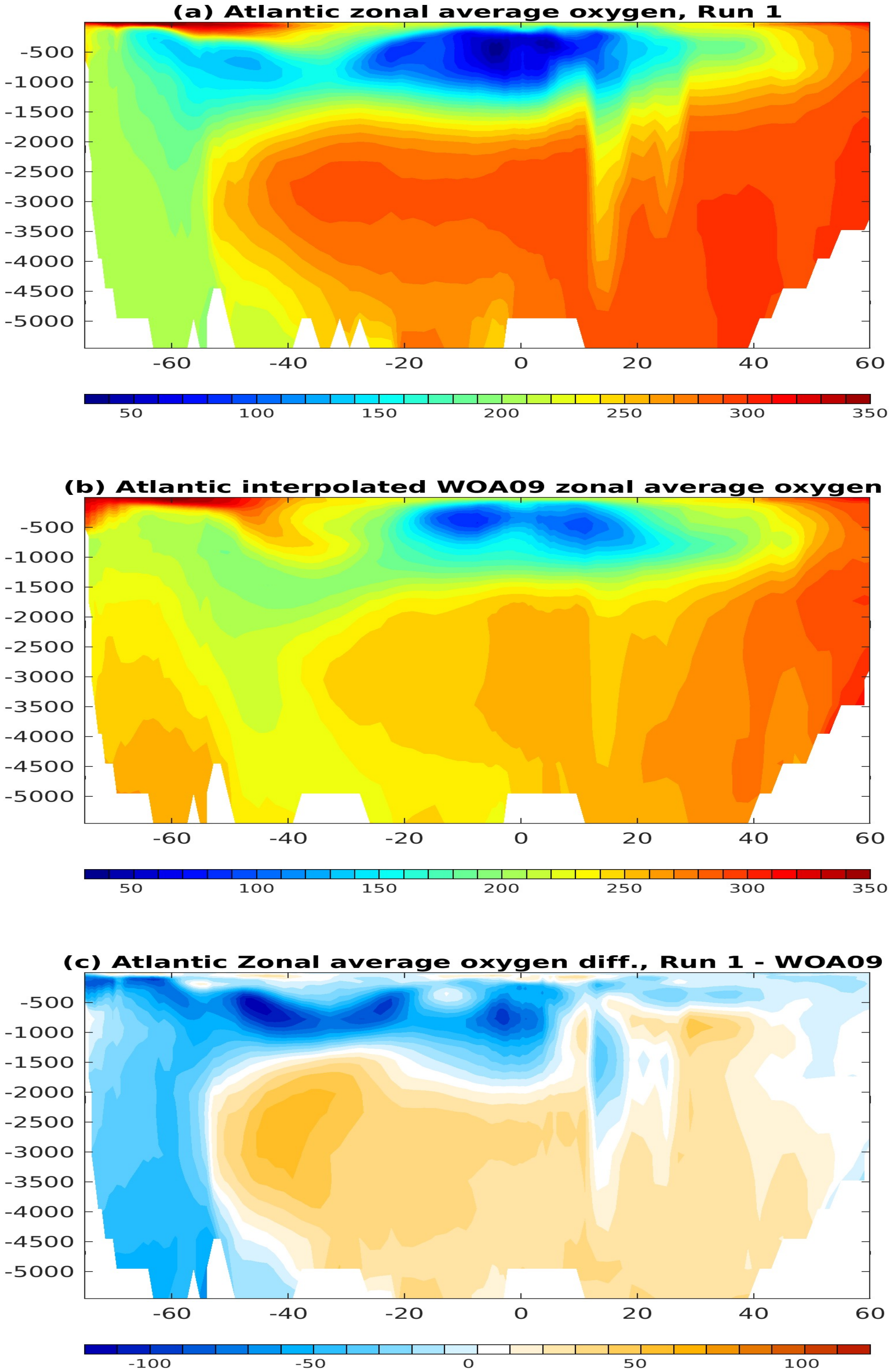

Figure 3.8: *Zonal averaged Atlantic oxygen for model(a), interpolated WOA09(b) and their differences(c)* ($\mu mol L^{-1}$)

higher oxygen concentration which decreases as the water mass flows southward to the Southern Ocean. This may be attributed to the fact that the NADW is relatively cold and fresh in the observation.

Model - observational data plot shows negative values in the high latitude North and South Atlantic, AAIW, AABW, the thermocline region in the tropics and subtropics and the whole of the Southern Ocean. This may be attributed to the somewhat warm and saltier WOA09 compared with the model. The NADW has a positive difference which increases as the water mass flows southward signifying the availability of more dissolved oxygen in the model than the observational data. This is also consistent with the explanation that the remineralisation occurs at the subsurface more than in the deep ocean. This makes the nutrient concentration to be less in the deep ocean and hence higher oxygen.

3.2.4 Pacific zonally averaged nitrate

The Pacific ocean zonally averaged nitrate is presented in Figure 3.9. For the model nitrate as presented in Figure 3.9a, the nitrate concentration is fairly constant in the Southern Ocean, between approximately 70°S - 60°S through the water column. Holm-Hansen (1985) also described the uniformity by the upward mixing and upwelling of nitrate. The AAIW which moves northward in the Pacific Ocean is also nitrate-rich. There is an upwelling of nitrate concentration below the surface water at the equator. The thermocline waters in the subtropical gyres have low concentrations at depth due to downwelling of nutrient-poor waters (Reid Jr 1962). The low surface nitrate in the South Pacific extends up to about 700m deep between 60°S - 20°S as compared with the low nitrate layer in the North Pacific which extends up to about 600m deep. The maximum nitrate can be seen at the NPW and NPIW waters between 35°N - 60°N. The maximum at the mid-latitudes in the North Pacific is connected with the PDW. There is also a decrease in nitrate concentration from north to south in the deep Pacific Ocean.

For the interpolated WOA09 zonally averaged nitrate in the Pacific, the tropical and subtropical gyres are depleted in nitrate at the surface but it is thin at the equator due to the nitrate-rich waters beneath it as shown in Figure 3.9b. The intrusion of old aged NPIW and NPDW comes with the highest nitrate located at the northern mid-depth between 20°N - 50°N. The nitrate also decreases as the water mass flows from north to the south in the deep ocean and shows constant distribution. The SPIW and the entire Southern Ocean has a little bit high oxygen which is also fairly distributed through the water column.

The model-observational data difference zonally averaged nitrate in the Pacific is shown in the bottom figure of Figure 3.9. The SPIW shows negative nitrate differences signifying high observational nitrate values compared with the model

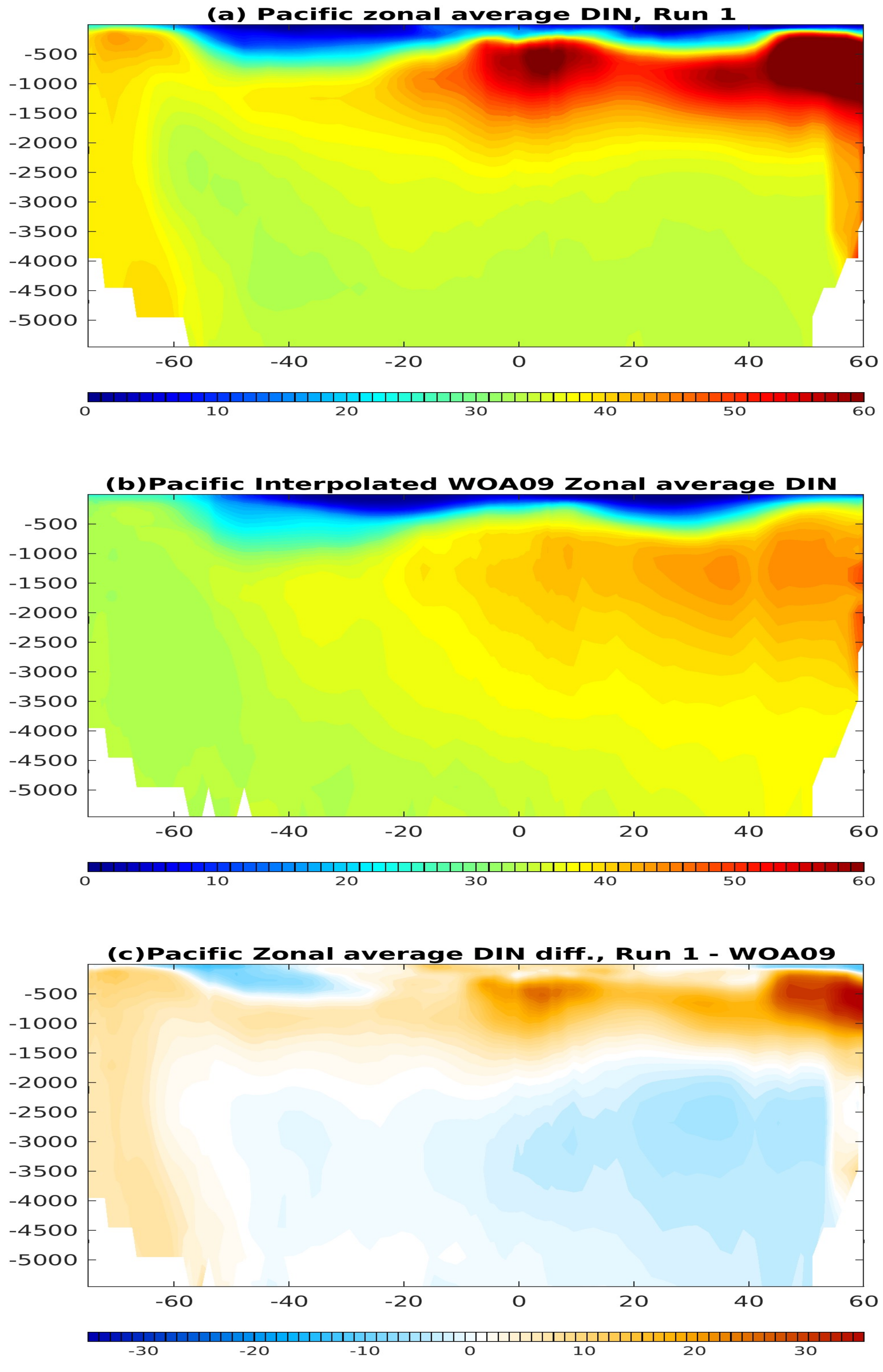

Figure 3.9: *Zonally averaged Pacific DIN for model(a), interpolated WOA09(b) and their differences(c)* ($\mu mol L^{-1}$)

value. The deep oceans have also a negative anomaly and increases as the water mass flows northward. The high positive difference values can be seen at NPIW, the equatorial waters in the tropics and subtropics and the entire surface waters except for the SPIW intrusion and in the Southern ocean.

3.2.5 Pacific zonally averaged oxygen

The oxygen concentration in the Pacific is seen to be associated with some major water masses as shown in the right column of Figure 3.10. The main water mass features are shown are the SPIW, AAIW, NPDW and the PIW. The upper right figure shows the zonally averaged dissolved oxygen in the Pacific Ocean for the model. The Pacific surface water and the SPIW are very rich in oxygen concentration. This is similar to the AAIW at the South Atlantic where the cold oxygen-rich Antarctic surface water meets warm and salty sub-Antarctic surface waters. The Southern Ocean show slightly low oxygen content but gradually increases as it gets to the sea floor. Similar processes lead to the formation and maintenance of the South Atlantic and South Pacific due to the resemblance in their deep oxygen minimum. The old aged NPIW and NPDW have the lowest oxygen concentration in the Pacific Ocean at mid-depth. This minimum oxygen concentration can be attributed to the North Pacific circulation system in which oxygen reduces away from the source and the replacement by vertical diffusion. The equatorial subsurface tropics and subtropics also have an oxygen minimum zone. The bottom waters between $3000m$ to the abyss shows slight maximum oxygen concentration probably due to bottom current.

The interpolated observational data zonally averaged dissolved oxygen in the Pacific Ocean is shown in the middle figure also shows some features similar to that of the model. The southern sourced AAIW and the surface waters have the highest oxygen concentration in the Pacific Ocean. The Sothern Ocean has slightly high oxygen concentration which increases proportionally with depth. The NPIW and the NPDW have the lowest dissolved oxygen zone but show an increase in concentration from north to south. Generally, the deep and bottom waters increase from the North to the South Pacific.

The difference in the model and observational data is shown in the bottom right figure. There is negative oxygen anomaly at the surface of the Pacific Ocean at the high latitudes, the SPIW and the Southern Ocean. There is a positive anomaly at the surface water and the deep ocean signifying high model oxygen concentration. The SPDW has slight negative values which decrease further with depth and also with the water flowing from south to north. All these are associated with cold and less saline observational data at these regions.

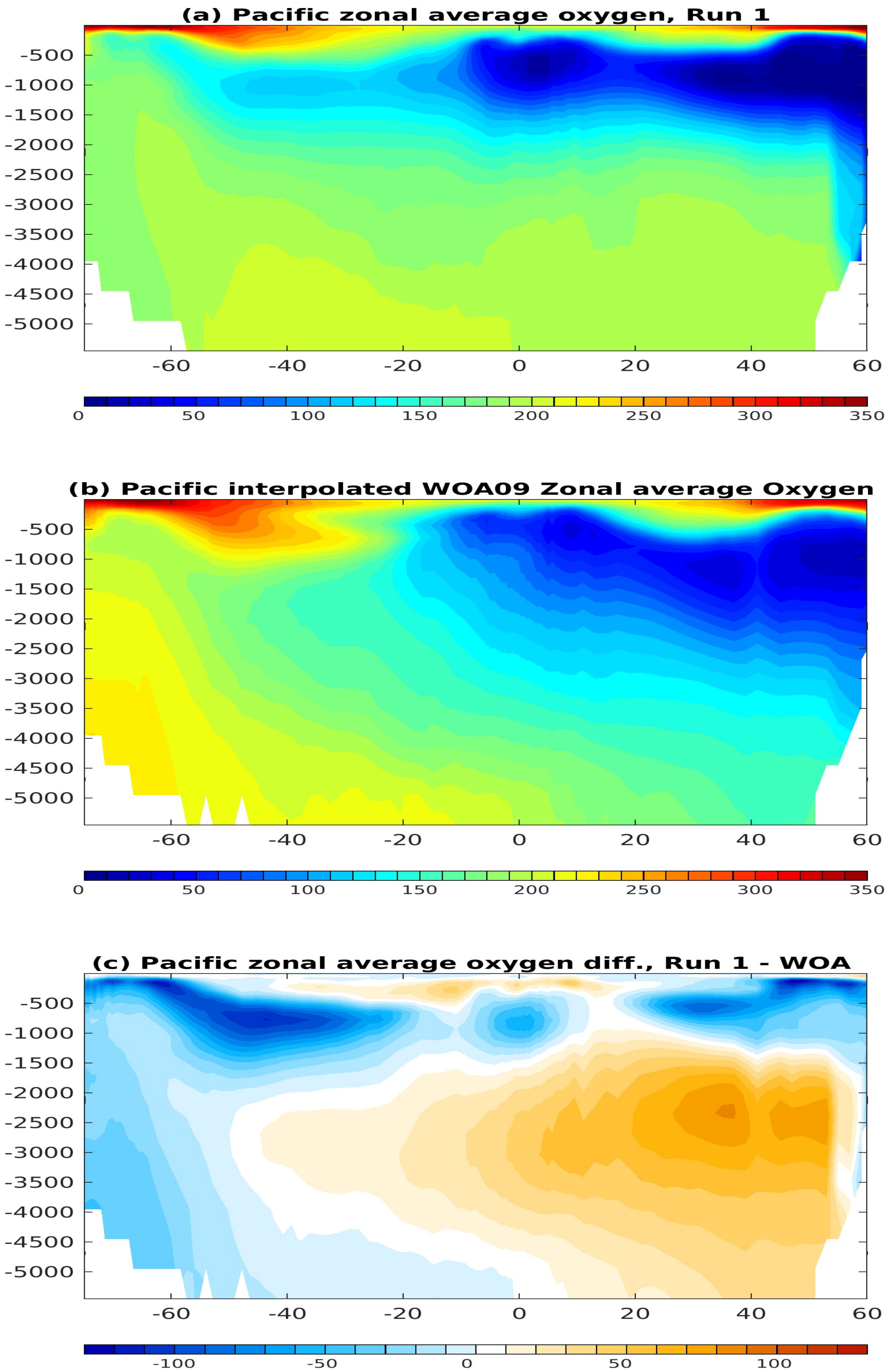

Figure 3.10: *Zonally averaged Pacific oxygen for model(a), interpolated WOA09(b) and their differences(c)* ($\mu molL^{-1}$)

Chapter 4

Results from sensitivity model runs

To examine how some parameterisation of physical and biological processes affect the temperature, salinity, oxygen and nitrates distribution in the Atlantic and Pacific Ocean, several modifications were made in the model, compared to standard model run. These changes includes: Increasing and decreasing the diffusivity rate constant in the Gent-McWilliams parameterisation as shown in Table 2.1, changing the topography in the Denmark Strait to make it shallower to allow the overflow of water from the Greenland Sea to the North Atlantic, increasing the vertical gradient of the sinking speed of particles by 11.11% and 50% and decreasing the remineralisation rate constant for nitrogen and carbon by 13.3% and 26.6% as shown in Table 2.1. Here we show the difference between zonal averages of temperature, salinity, nitrate and oxygen for each of the modified model run and the standard or reference model runs to describe the changes that occur of the sensitivity experiments. In the physical model section we show only the effects for runs 2 to 4 since runs 6 to 9 have the physics unchanged. Runs 6 to 9 also do not have oxygen module of the model oxygen switched on so we compared only nitrate.

4.1 Physical model

4.1.1 Atlantic zonally averaged temperature difference

The upper figure in Figure 4.1 shows the difference between the model run with decreased GM diffusivity rate constant and the standard model in the Atlantic. There is a positive anomaly in almost all the entire Atlantic Ocean basin. This means that decreasing the GM diffusivity rate constant results in a temperature

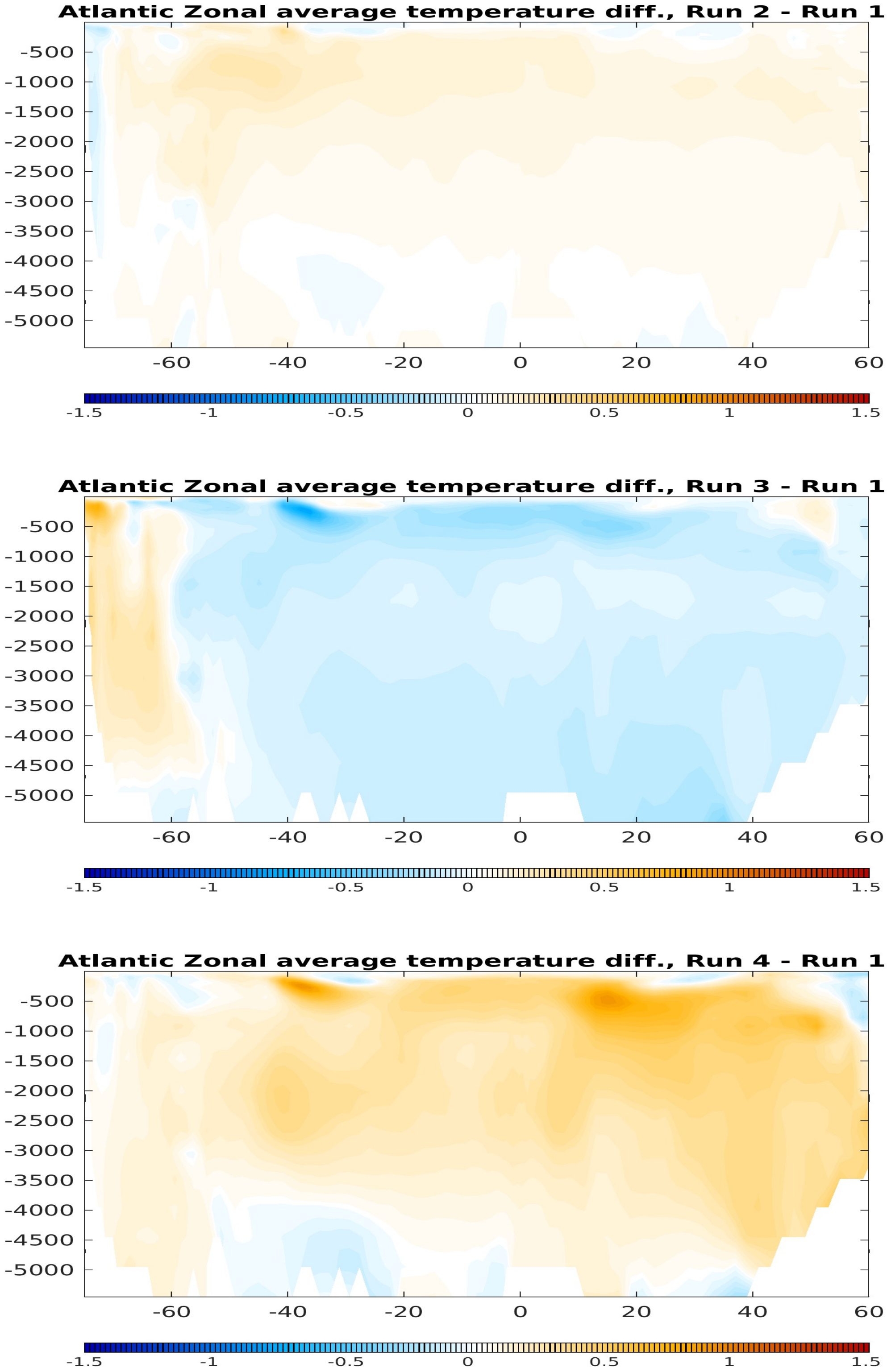

Figure 4.1: *Zonally averaged Atlantic temperature difference for simulated model runs compared to the standard model run (simulated model run − standard model run), (°C)*

increase of all the Atlantic deep water masses.

In contrast with the above, increasing the GM diffusivity rate constant (Figure 4.1 middle) results in a negative anomaly in most of the water masses except the South Atlantic high latitude surface waters and the AABW which have a positive temperature anomaly. This means that the modified modelled run results in an increase in temperature in AABW and the southern high latitude water, but the rest of the Atlantic Ocean decreases.

Changing the topography in the Denmark Strait Figure 4.1 lower panel) also results in a positive anomaly in almost the entire Atlantic Ocean. This implies that shallowing the topography the Denmark Strait also increases the temperature of Atlantic ocean waters.

4.1.2 Atlantic zonally averaged salinity difference

The salinity in the Atlantic Ocean is also affected by the changes in the standard model as shown in Figure 4.2. The anomaly is between -0.2 and 0.2.

In the upper figure, there is a slight change in the salinity level in the Atlantic Ocean when the diffusivity rate constant was decreased. A clear difference is a positive change in the South Atlantic water signifying increasing the salinity at that region in the sensitivity run but the rest do not show any appreciable anomaly. The maximum salinity anomaly is around 0.01.

In the middle figure increasing the diffusivity constant slightly change the salinity level but the magnitude is a little bit higher than the decreasing the diffusivity rate. A positive anomaly in the South Atlantic represents increasing salinity at that region in the sensitivity run (less than 0.1). The rest of the Atlantic show negative difference which means the modified model water is freshened (less than 0.1).

When the Denmark Strait topography is modified, the salinity is increased. This is the reason we have a positive anomaly in the whole Atlantic Ocean except in the AAIW where the water mass is freshened due to the changes.

4.1.3 Pacific zonally averaged temperature difference

The temperature in the Pacific Ocean is also affected by the changes in the physical processes. The change is generally smaller in the Pacific as shown in Figure 4.3 (between -0.3K and 0.3K).

The upper figure shows a slight negative anomaly in the SPIW, PBW and the NADW (all less than -0.05K) representing a decrease in the water temperature in these regions when the GM parameterisation diffusivity rate was decreased. The temperature of NPDW increases as it flows southward. The surface and

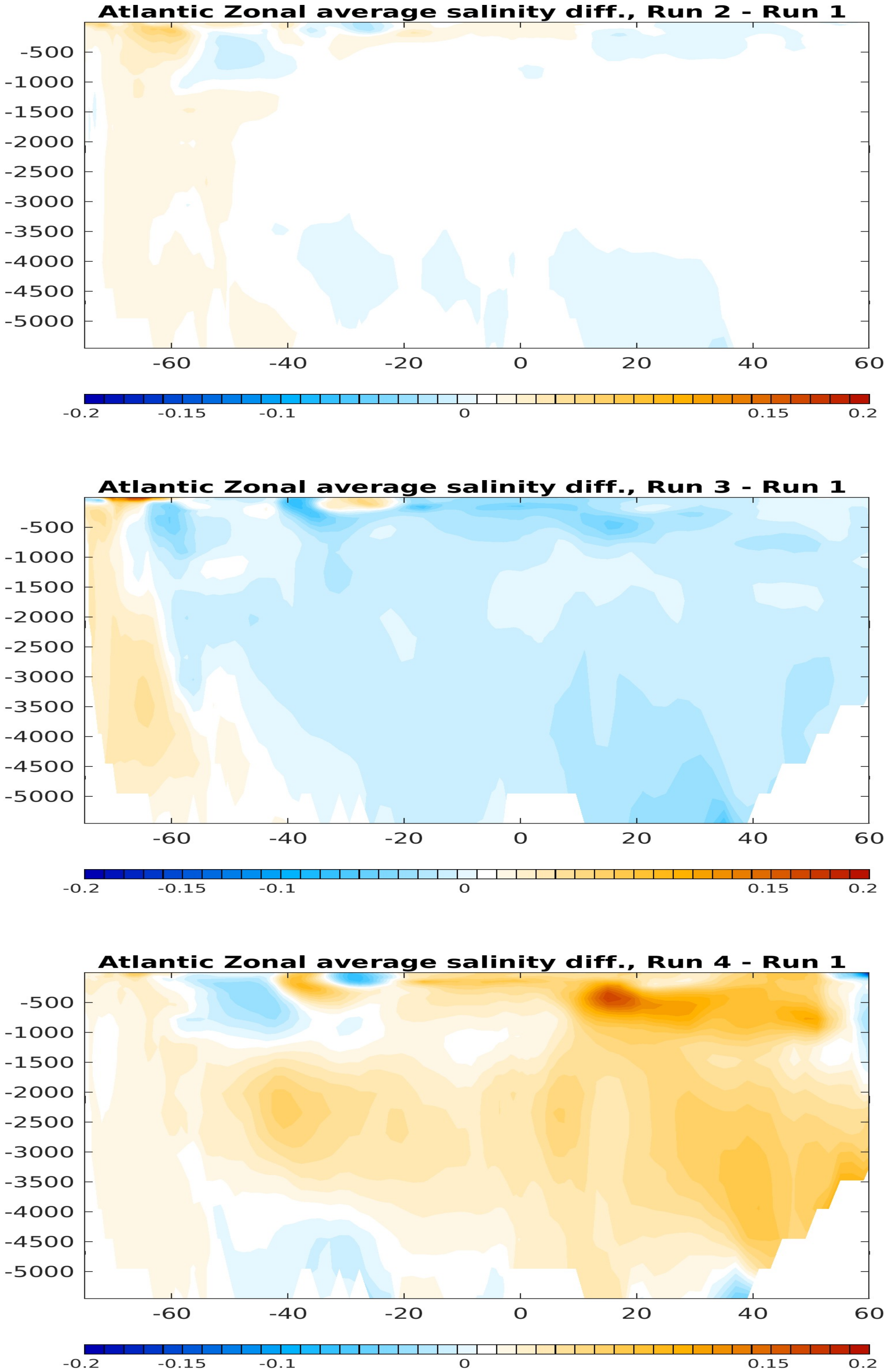

Figure 4.2: *Zonally averaged Atlantic salinity difference for simulated model runs compared to the standard model run (simulated model run − standard model run.)*

the subsurface Pacific Ocean have positive temperature anomaly (less than $0.1K$) signifying an increase in the temperature in the model run.

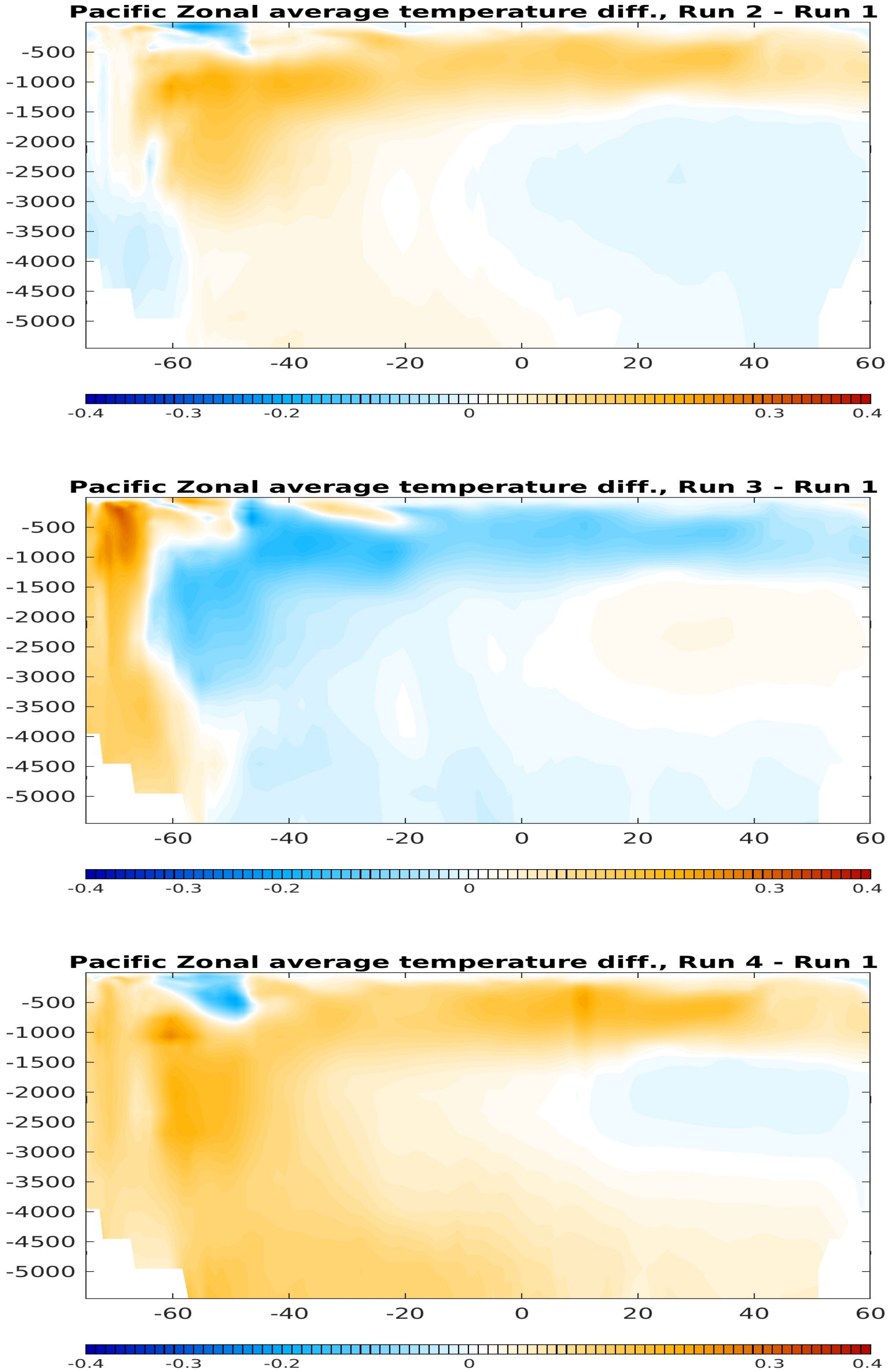

Figure 4.3: *Zonally averaged Pacific temperature difference for simulated model runs compared to the standard model run (simulated model run − standard model run) (°C)*

In increasing the GM diffusivity rate in the middle figure, the South Pacific

Ocean has high positive temperature anomaly (less than $0.3K$) indicating an increase in the South Pacific water as the modification is made. The NPDW also has a positive difference and reduces little bit in the bottom waters and the Southern Ocean. The negative anomaly means a reduction in the temperature of this sensitivity experiment.

In the bottom figure, the entire Pacific Ocean shows a positive anomaly except for the SPIW. The positive temperature difference denotes an increase in the water temperature when the sill depth of the Denmark Strait is shallowed to allow the overflow of water from Greenland Sea while the temperature in the SPIW is reduced.

4.1.4 Pacific zonally averaged salinity difference

The salinity in the Pacific Ocean is also affected by the changes in the physical processes. The change is not very profound as shown in Figure 4.4 (between -0.1 and 0.1).

The South Pacific high latitude, deep and bottom water has positive salinity anomaly (up to about 0.04) and the North Pacific extending to the subtropics have negative salinity differences. This means there is an increase in salinity in the Pacific water where the anomaly is positive and freshening where the anomaly is negative when the diffusivity rate is reduced in the upper figure.

The pattern is reversed when the diffusivity is increased. The South Pacific high latitude, deep and bottom water has negative salinity anomaly (up to about -0.1) which denotes the freshening of the water in these regions and the North Pacific extending to the subtropics have positive salinity differences (less than 0.04) signifying the water in these regions becoming saltier.

The bottom figure shows negative salinity anomaly (less than -0.05) in the North Pacific. This anomaly decreases with depth and from north to south. This represents a decrease in the salinity in this region. The South Pacific is characterised by high anomaly (less than 0.04) indicating the salinity increases as the topography in the Denmark Strait is modified.

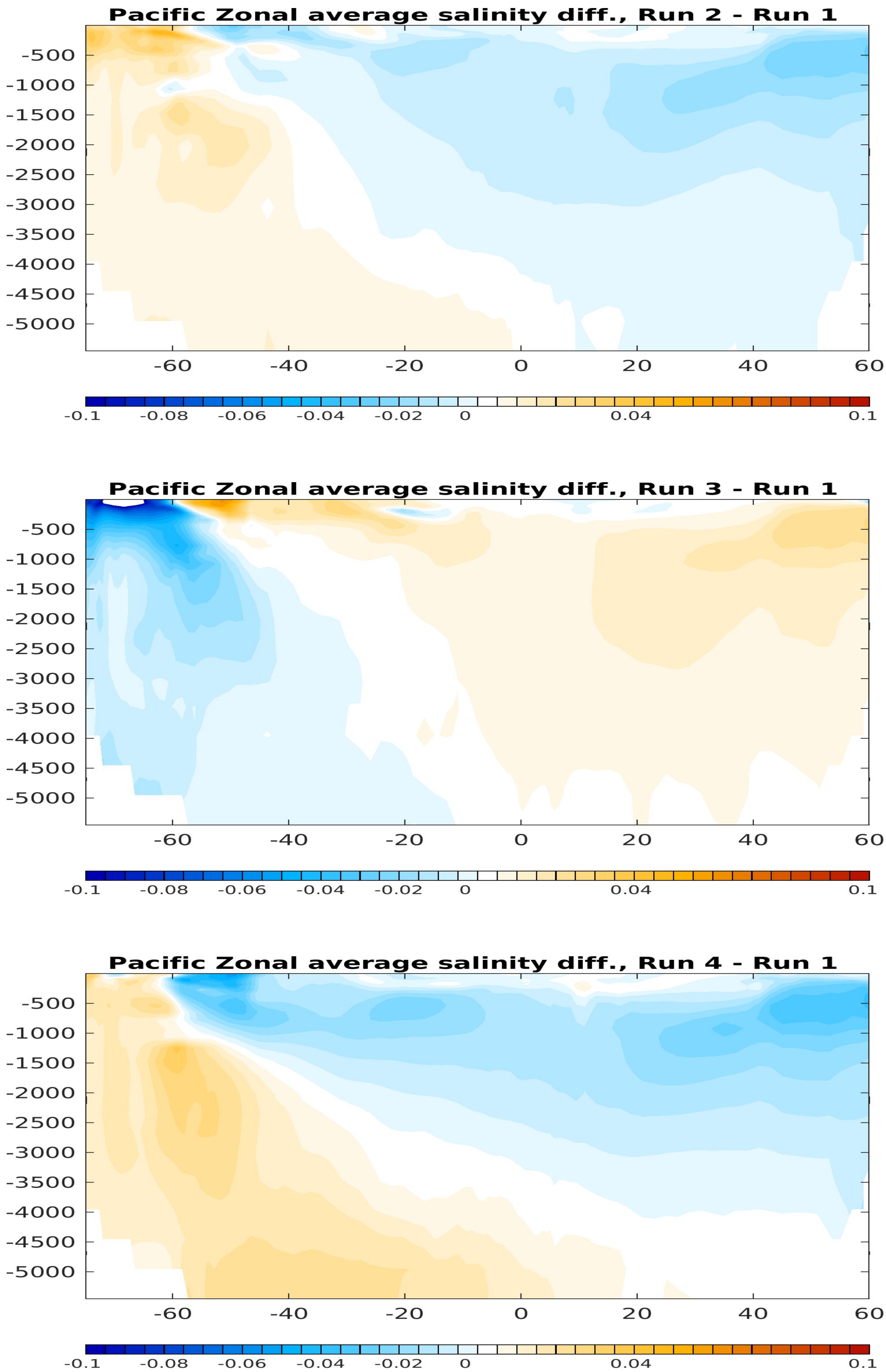

Figure 4.4: *Zonally averaged Pacific salinity difference for simulated model runs compared to the standard model run (simulated model run − standard model run.)*

4.2 Biogeochemical model

4.2.1 Atlantic zonally averaged nitrate

In comparing the effect of the modifications made in the sensitivities model runs, differences between the simulated model runs and the standard models are shown in Figure 4.5.

Figure 4.5 (upper) did not show much difference between the reduced diffusivity constant in the GM parameterisation simulated model run and the reference run. There are very little negative differences in the southern high latitude and the South Atlantic deep and bottom waters between about -1$\mu mol L^{-1}$ to -3$\mu mol L^{-1}$ and 1$\mu mol L^{-1}$ to 3$\mu mol L^{-1}$ in the subtropics. This means reducing the effect of the non-resolved-eddies in the model did not have a significant change in the DIN distribution.

The middle figure of Figure 4.5 shows a slight negative anomaly in the South Atlantic bottom waters and slight positive anomaly at the subtropics covering very small regions. This represents the effect of the increase in the diffusivity constant in the GM parameterisation. This also does not have any major impact on the distribution and concentration of the nutrients in the Atlantic ocean.

The third figure at the bottom of Figure 4.5 represents the differences between the model run with modified Denmark strait topography and the reference model. This shows an appreciable anomaly in the Atlantic Ocean. The negative anomaly at the upper layers of the subtropics, tropics and the North Atlantic extends up to about 2000m and 50°S to 60°N. between 50°S - 40°N the bottom there is a positive anomaly in bottom waters. The DIN concentration in the mid-depth throughout the Atlantic is a little bit higher in the modified topography change. This shows that changing the sill depth in the Denmark Strait affects the distribution of the DIN in the Atlantic Ocean.

4.2.2 Atlantic zonally averaged oxygen

Unlike the nitrate distribution anomaly in the Atlantic ocean, there are clear deviations between all the simulated model runs and the standard run as shown in Figure 4.6.

When the GM diffusivity constant is decreased the distribution of oxygen is altered. The Southern Ocean show uniform high anomaly value between 70°S - 40°S. This means the oxygen concentration decreases in this region in the modified run. The rest of the Atlantic Ocean shows decreased oxygen concentration in the modified model run. This results in a negative anomaly with the lowest values in

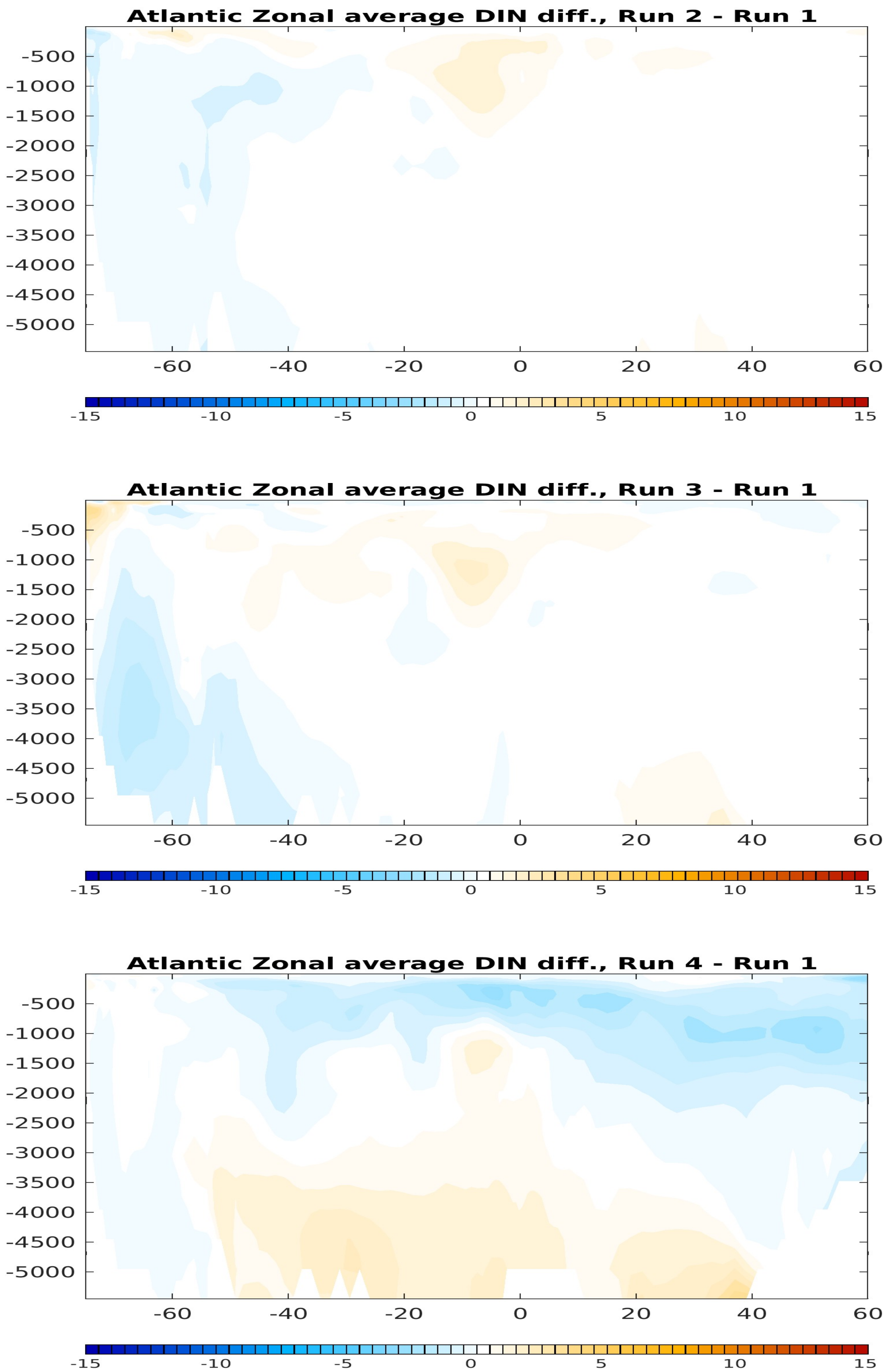

Figure 4.5: *Zonally averaged Atlantic DIN between simulated model runs and the standard model run (simulated model run − standard model run.) for physical simulation*$(\mu mol L^{-1})$

the subsurface of the subtropics and the AAIW.

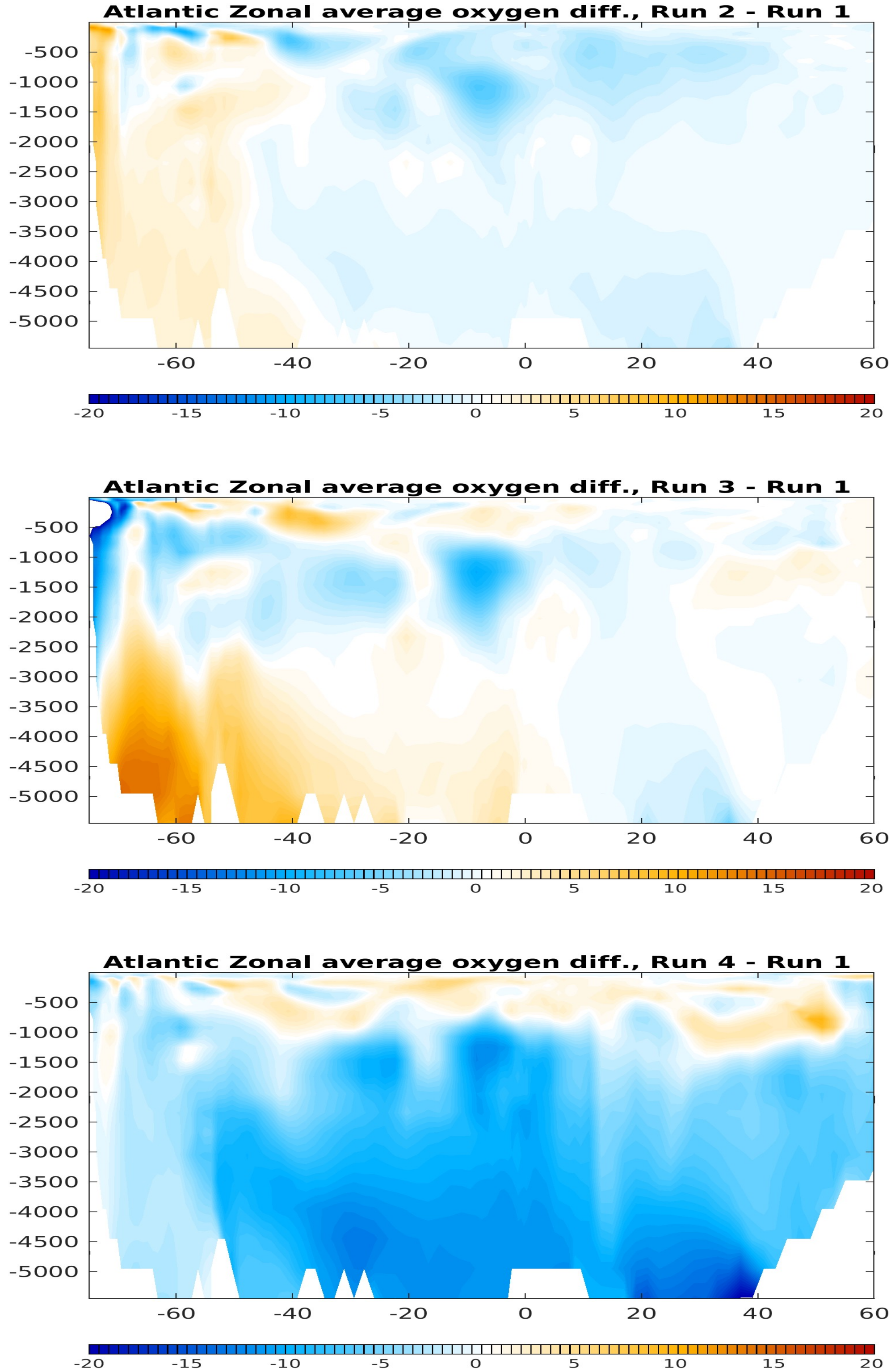

Figure 4.6: *Zonally averaged Atlantic oxygen between simulated model runs and the standard model run (simulated model run − standard model run.) for physical simulation*($\mu mol L^{-1}$)

However, when the diffusivity rate constant in the GM parameterisation is increased, the deviation was higher as shown in Figure 4.6(middle) than when it was reduced. The deviations are generally high with some small regions with low anomaly. The bottom waters at the South Atlantic have increased in oxygen concentration and the far left of the upper left South Atlantic are the notable ones. All the modification led to the increase in oxygen in the Atlantic ocean.

The bottom figure shows a clearer view of the anomaly. The upper 500m is generally rich in oxygen and the whole of the deep and bottom water in the Atlantic Ocean shows a reduction in oxygen. This resulted in the high oxygen deviation at the surface and very low in the deep and bottom waters, with the anomaly decreasing with depth. This implies that changing the topography of the Denmark Strait by increasing the sill depth increases the simulated model run oxygen concentration at the surface and reduces the oxygen in the deep and bottom waters as compared with the reference model run.

Atlantic zonally averaged nitrate for biogeochemistry modification

The differences between the Atlantic sensitivity model run and the standard model run are shown in Figure 4.7. From model Run 5 to Run 9, there is a common pattern which is a decrease in DIN in the subsurface of the Atlantic Ocean especially very strong in the upper 1000m where remineralisation occurs most and weaker in the deep ocean. All these runs decrease the release of nutrients in the upper water column and increase it in the lower column. This decreases the nutrient concentration everywhere in the upper water column and somewhat in the new water formed in the Atlantic ocean. Although all the model runs have a quantitatively similar effect, the amplitude is different between the model runs. Comparing the model runs, Figure 4.7a which has the smallest remineralisation constant had the greatest in nitrate.

In accordance with Figure 4.7, it can be deduced that changing the sinking speed and remineralisation of nitrates in the Atlantic Ocean directly affect its distribution. Figures 4.7a and 4.7c are the models run with an increase in the vertical gradient of sinking speed by 11.11% and 50% respectively. The higher the increment in this gradient, the higher the sinking speed according to the equation 2.8 . Comparing these two models with the standard model run, we could see that Figure 4.7a has more nitrate available at the remineralised upper sub-tropic region since the sinking speed was increased. This causes less organic nitrogen to be transported to the deep ocean. This is the reason there is a little bit lower negative anomaly in the remineralisation zone signifying higher nitrate in the standard model and an increase in the deep ocean since the mid-depth and deep nitrate concentration has been slightly increased due to the increment in the sinking speed. For Figure 4.7c, the vertical gradient of sinking speed is highly increased. Since more nutrient is able to sink from the remineralised upper tropics and subtropics region, less nitrate will be available at the surface and more in the deep ocean. This is the reason we have an extremely high negative anomaly in the subtropics.

The model's rate of remineralisation was also altered in the course of this study. Figures 4.7b and 4.7d represent the model run with the remineralisation rate modification in the Atlantic Ocean. These two figures saw the remineralisation rate reduced by 13.3% and 26.6% respectively. The higher the magnitude of the remineralisation rate reduction the deeper the particle sinks before remineralised into the ocean.
Run 7 has the least reduction among the two which means more nitrates will be released into the ocean than model Run 9.

The remineralisation region in the subtropics shows high negative anomal and slightly low in the upper surface of Figure 4.7b whereas Figure 4.7d reproduced higher negative anomaly in the same region. This shows the nitrate concentration is reduced when the remineralisation rate is reduced which reduces the resupply of nutrient. This makes the nitrate concentration higher in the model than in model Run 7 and much higher than in model Run 9.

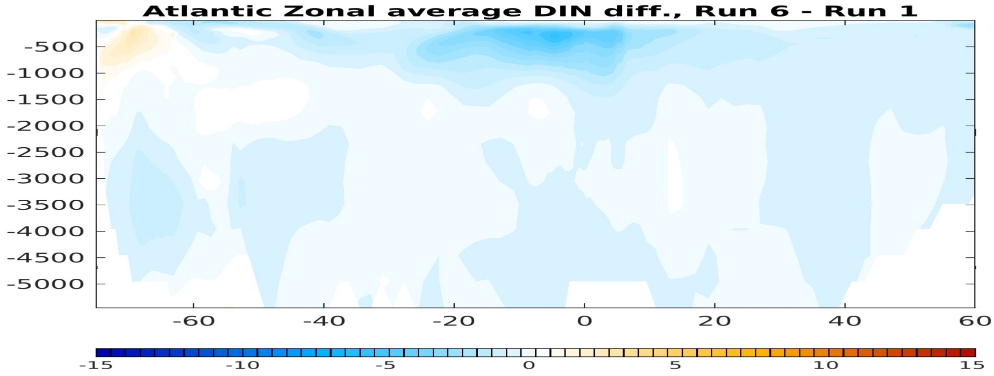

(a) *Model run with 11.11% vertical gradient reduction – Standard run*

.

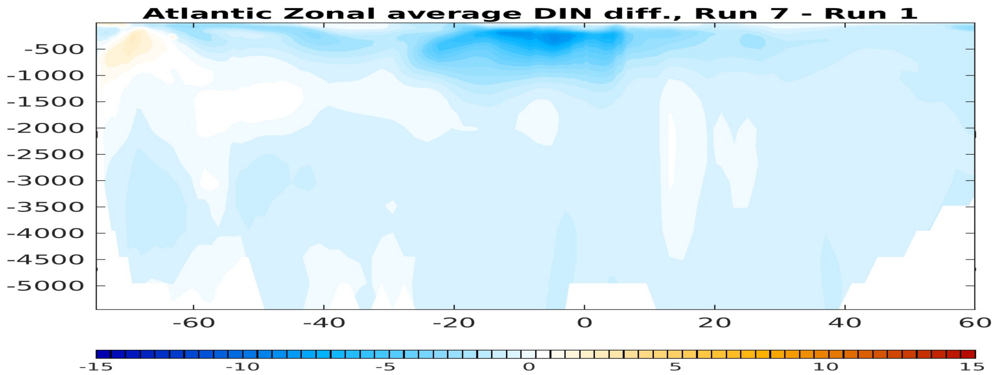

(b) *Model run with 13.3% remineralisation constant reduction – Standard run.*

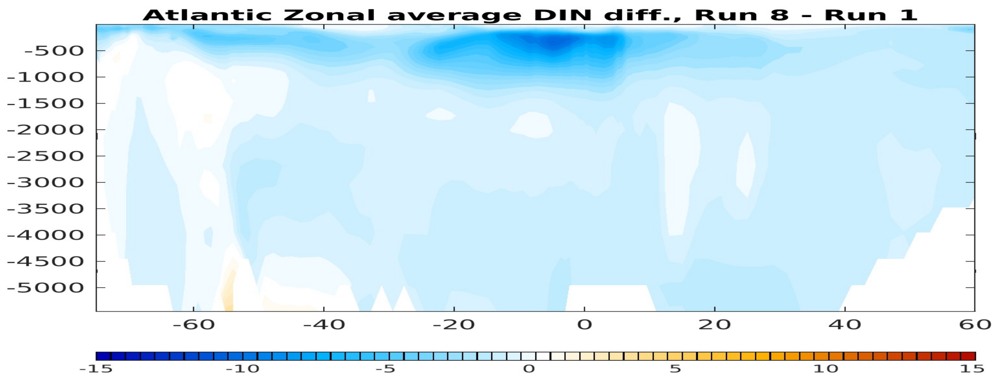

(c) *Model run with 50% vertical gradient reduction – Standard run.*

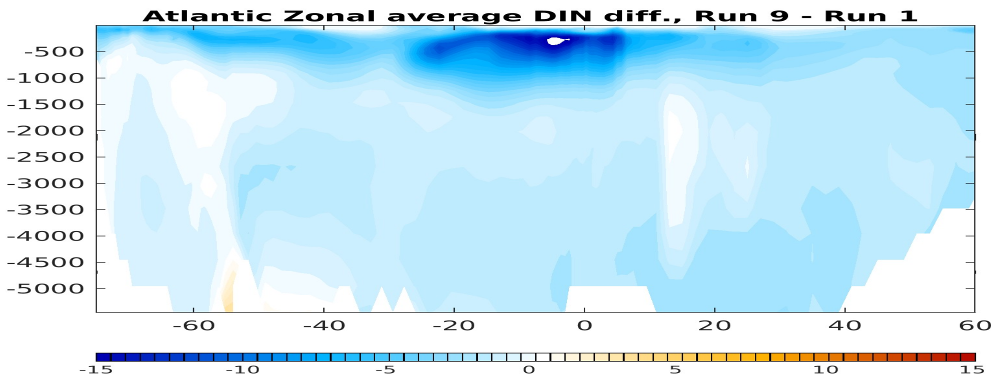

(d) *Model run with 26.6% remineralisation constant reduction – Standard run.*

Figure 4.7: *Atlantic biogeochemical simulated model runs and Standard run differences* ($\mu mol L^{-1}$)

4.2.3 Pacific zonally averaged nitrate

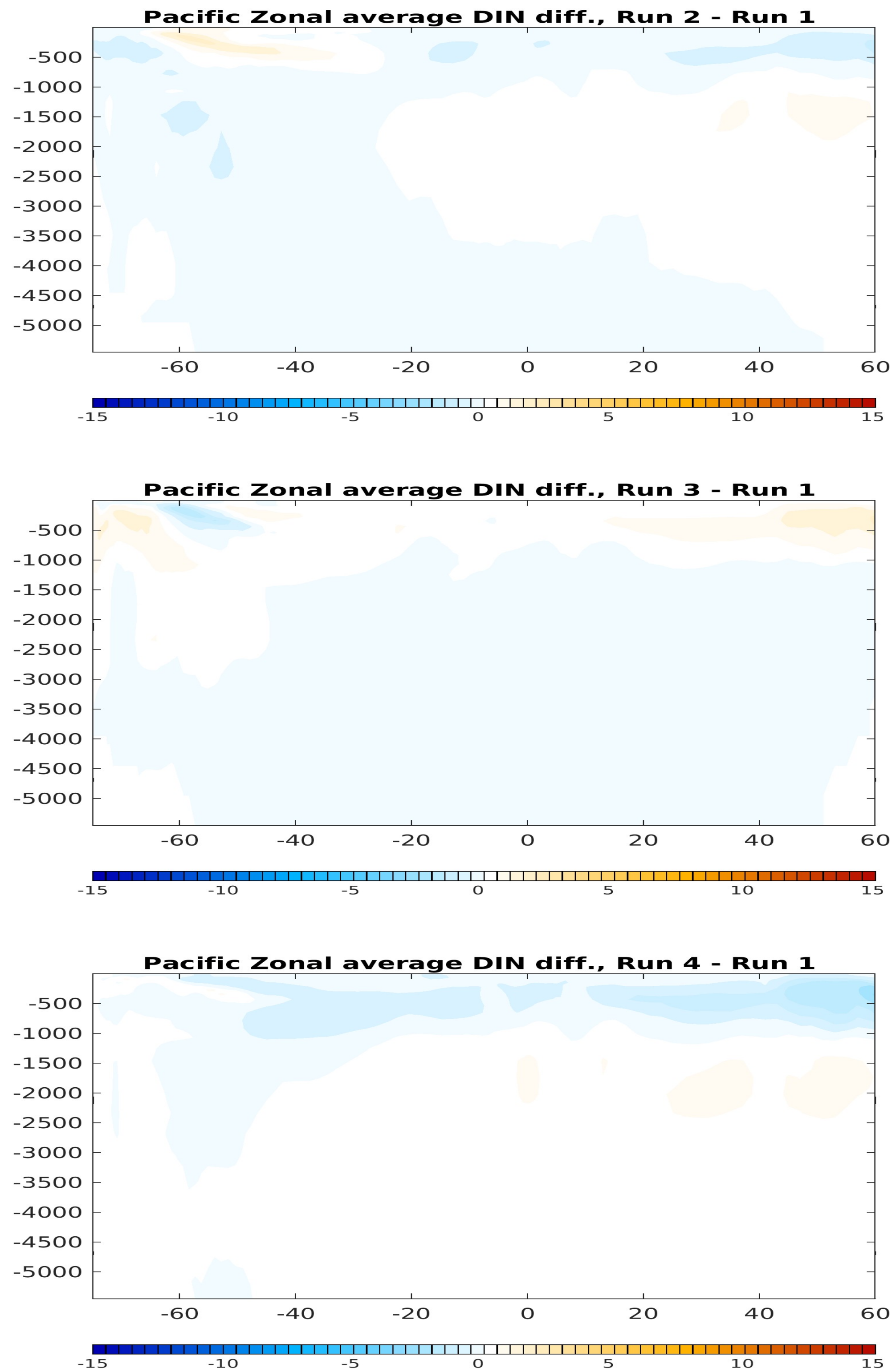

Figure 4.8: *Zonally averaged Pacific DIN difference between simulated model runs and the standard model run (simulated model run − standard model run.) for physical simulation*($\mu mol L^{-1}$)

The Pacific DIN difference between the physically simulated model runs and the standard model run in the Pacific ocean are shown in Figure 4.8.

In the first figure, reducing the GM parameterisation diffusivity rate constant reduces the DIN concentration in most part of the Pacific Ocean by less than $1 \mu mol L^{-1}$. This is seen in the negative anomaly at the most part of the surface, bottom and South Pacific deep waters. But the same effect increases the DIN concentration in the SPIW and the old aged Pacific deep water for the simulated model run. This therefore results in a positive anomaly in the SPIW and old age Pacific deep waters.

By increasing the GM diffusivity rate constant, the DIN concentration in the Pacific Ocean increases in the surface waters at the tropics, subtropics and the north and south high latitudes except in the PIW which is DIN depleted in the modified model run as seen in the middle figure. However, the reverse takes place in the deep and bottom Pacific waters where the DIN in the water is reduced as compared with the standard run. Increasing the diffusivity rate constant produces a high negative anomaly (-2 $\mu mol L^{-1}$) in the SPIW and low negative deviations (-0.5 $\mu mol L^{-1}$) in the deep and bottom waters, denoting high DIN in the referenced model run or reduced DIN in the simulated run. A high positive (1 $\mu mol L^{-1}$) in the NPIW, the surface of the tropics and the southern high latitude waters below the SPIW (less than 0.5 $\mu mol L^{-1}$) shows increased nitrate in the model relative to the reference model run.

When the sill depth is increased in the Denmark Strait, the Pacific Ocean has increased DIN in the SPIW and the South Pacific deep and bottom waters and also south of the Pacific deep and bottom waters between $1100m$ which is reduced as the water flows southward and downward as shown in Figure 4.8 (middle). This changes also resulted in the decrease in the DIN concentration at the surface and subsurface waters in the Pacific ocean. Changing the topography in the Denmark Strait results in a very high negative anomaly in the surface and subsurface of the Pacific with the highest amplitude in the NPIW (greater than -2 $\mu mol L^{-1}$) denoting a reduction in DIN in the simulated model run. Also, the deep, bottom and southern high latitude Pacific waters show high positive anomaly with the maximum value around 0.8 $\mu mol L^{-1}$ in the Pacific old aged water.

4.2.4 Pacific zonally averaged oxygen

The Pacific Ocean oxygen concentration was also affected when the standard model was modified as can be seen in Figure 4.9.

Decreasing the GM parameterisation diffusivity rate constant, the modified

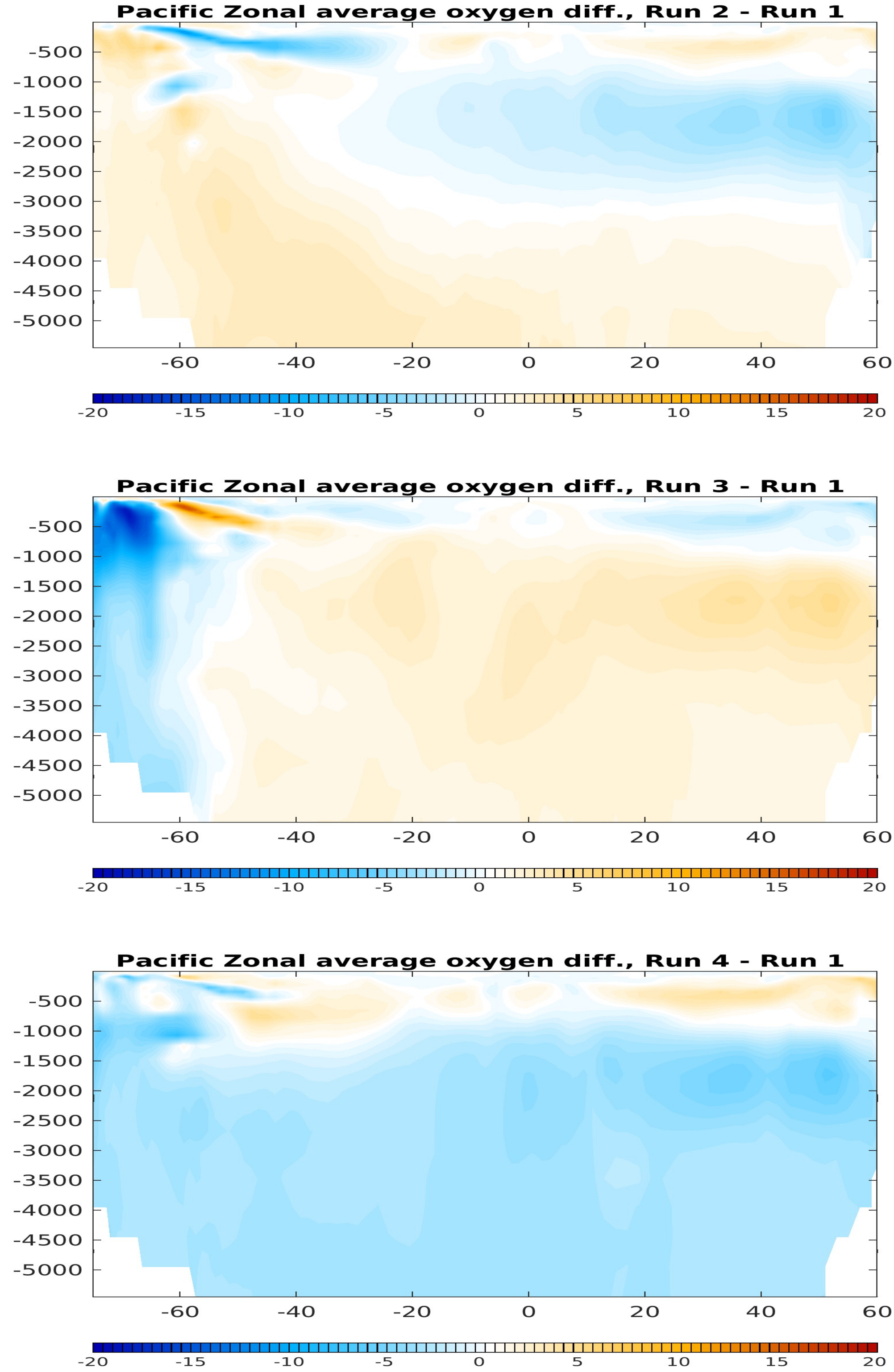

Figure 4.9: *Zonally averaged Pacific oxygen difference between simulated model runs and the standard model run (simulated model run − standard model run.) for physical simulation*($\mu mol L^{-1}$)

modelled run had an increase in the most part of the Pacific Ocean including the SPIW, PBW and NPBW except in the SPIW and the mid-depth old age waters between 30°S – 60°N and extending between $1000m$ and $3000m$ deep. This accounts for why there are high oxygen anomaly in the SPDW, NPBW and PBW and a negative anomaly in the SPIW and some part of the mid-depth Pacific Ocean.

The middle figure represents the effect of the increasing diffusivity rate constant in the GM parameterisation. There is a high positive anomaly in the SPIW and positive difference in the deep and bottom deep waters in the North Pacific and also at the subsurface low latitude tropics and subtropics. This means increasing the diffusivity rate constant increases the oxygen concentration in these regions of the Pacific Ocean. The high-latitude SPDW and SPBW and the surface of the ocean including the NPIW have a high negative anomaly with the minimum at the high latitude South Pacific surface. Meaning the modification depleted these regions with oxygen.

In modifying the topography of the Denmark Strait, the surface and subsurface Pacific Ocean have positive deviation extending up to about $1300m$. The high latitude South Pacific and the rest of the Pacific Ocean have a negative difference value. This is because changing the strength of the overflow by widening or changing the sill width, the surface and subsurface Pacific will have an increase in the oxygen concentration and the bottom, deep and the South Pacific high latitudes have the oxygen concentration decreased compared with the standard model.

4.2.5 Pacific zonally averaged nitrate, biogeochemical changes

Figure 4.10 shows the zonally averaged DIN for the differences between biological simulated model runs and the standard run in the Pacific Ocean. All the figures display a similar pattern in the Pacific Ocean just like in the Atlantic Ocean. Nitrates are generally reduced at the surface $500m$ and increase below especially in the Pacific deep waters. The increase is specifically in the old waters of the Pacific which has more time to accumulate.

For the increase in the vertical gradient of the sinking speed by 11.11% and 50%, i.e. Figures 4.10a and 4.10c respectively, both shows lower DIN difference at the surface which signifies faster transport of nutrients from the surface to the deep ocean. This makes the surface waters of the two models depleted in DIN. The standard model will have nutrient more than the simulated model runs. This explains why we have negative anomaly at the surface. This, however, explains why we have more nutrient in the model and hence the negative anomaly in these regions.

In the mid-depth, there is a high positive DIN anomaly in the Pacific Ocean unlike in the Atlantic. The water in this region is old and has already a high concentration of nutrient. As the surface water is depleted of nitrate by sinking faster in the simulated model, much of the nutrients are able to accumulate into an already existing nutrient-rich old aged water. The Figures 4.10a shows less positive anomaly since less nitrate to sink from the surface compared the that in Figure 4.10c which has very high positive anomaly because the sinking speed is higher than the former. Hence the nutrient concentration in the simulated models at the mid-depth is higher than that in the model. The two figures have similarly neutral anomaly at the South Pacific deep and bottom waters.

In Figures 4.10b and 4.10d, the remineralisation rate was reduced by 13.3% and 26.6% respectively. Since the regeneration of the nutrient into the ocean is reduced, the nutrient content or supply is also reduced. This is the reason the ocean surface has a negative anomaly for the two model runs with the later higher than the former since the reduction for the later is about double the former. The mid-depth has large positive anomaly between the older water mass nutrient concentration in the simulated models than the reference model run.

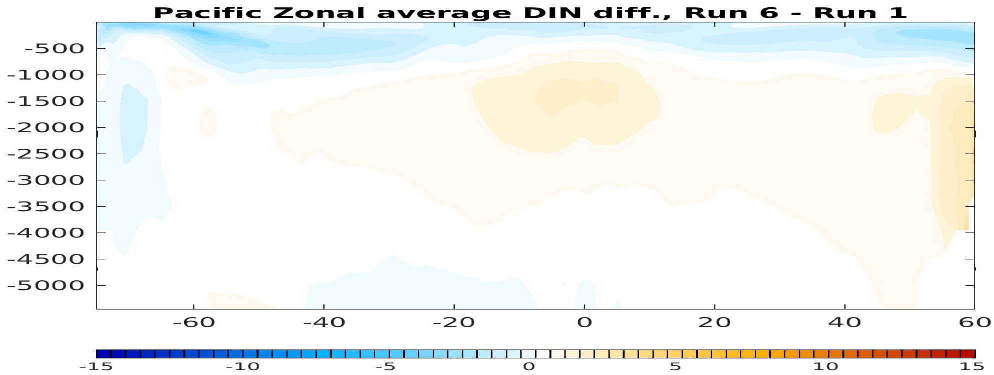

(a) Model run with 11.11% vertical gradient reduction − Standard run.

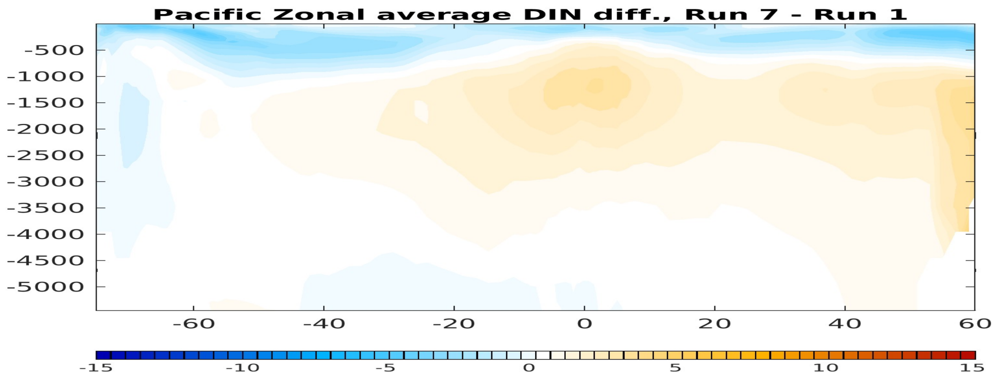

(b) Model run with 13.3% remineralisation constant reduction − Standard run.

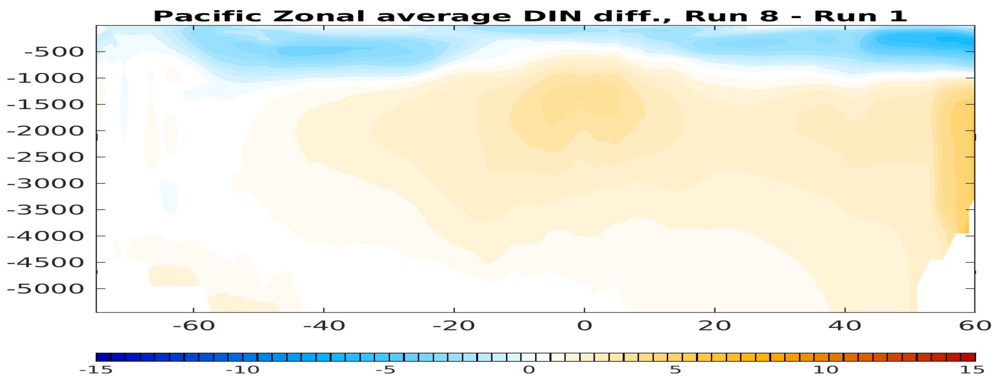

(c) Model run with 50% vertical gradient reduction − Standard run.

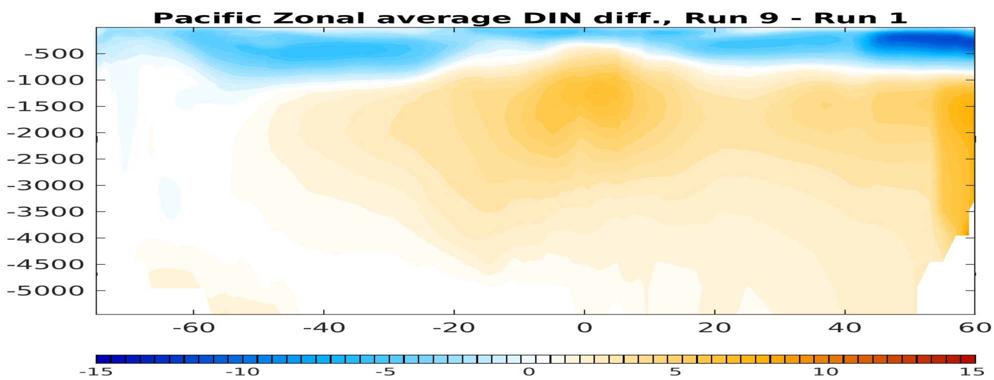

(d) Model run with 26.6% remineralisation constant reduction − Standard run.

Figure 4.10: *Pacific biogeochemical simulated model runs and Standard run differences* ($\mu mol L^{-1}$)

4.2.6 Physical model change

Measurements(Sv)	Run 1(Sv)	Run 2(Sv)	Run 3(Sv)	Run 4(Sv)
Overturning, 24°N	23.27	23.59	23.08	21.82
Min overturning, 26.5°N	-1.2	-1.6	-1.6	-2.0
Min overturning, 32°S	-2.70	-2.92	-2.35	-3.01
Drake Passage transport	133	139	124	138

Table 4.1: *Physical characteristics of the standard and sensitivity model runs.*

A comparison of the standard Run 1 to the Runs 2 - 4, where physical model settings have been changed, allows to identify a model run with improved circulation. Increasing and decreasing the diffusivity constant in the GM parameterisation respectively decreases (23.08Sv) and increases (23.59Sv) the Atlantic overturning strength even though the changes was not profound as can be seen in Table 4.1. However shallowing the topography of the Denmark Strait does have a relatively significant impact making the overturning strength more realistic. The maximum overturning at 24.5°N decreases to 21.8Sv, and the minimum overturning at 26.5°N decreases to -2.0Sv when the Denmark Strait was made shallower to decrease the strength of overflow from the Greenland Sea to the North Atlantic. These values are comparable to the observational RAPID data from Kanzow et al. (2010). In the sensitivity runs 2 - 3, the zero contour depth of the streamfunction remained unchanged, except the Run 4 which has it between 3400m to 3600m demonstrating a more realistic boundary between NADW and AABW.

The maximum transport between South America and the Antarctica (Drake Passage tranport) was also measured for the sensitivity experiments as shown in Table 4.1. An increase in the diffusivity constant in GM parameterisation and the modification of the Denmark Strait brought about an increase in the Drake Passage transport to 139Sv and 138Sv respectively which is very close to the 136.7 $\pm$ 7.8 Sv by Cunningham et al. (2003) and 140Sv by Ganachaud & Wunsch (2000). The increase in the diffusivity led to a reduction in the transport through the Drake Passage (124Sv) which disagrees with most measured values.

Chapter 5

Discussion

In chapter 4 we discussed how the modifications made changed the standard model run by comparing the sensitivity model runs to the standard model run. In this chapter, we discuss how well these sensitivity studies have brought the model closer to the observations. This can be measured by the RMSD, the bias and the correlation between the three dimensional annually averaged model fields and the annual average WOA09 fields. The statistics have been calculated using volume-weighted averaging, and the results are shown in Tables 5.1 through to 5.8.

	Run 1	Run 2	Run 3	Run 4
Bias($°C$)	1.383	1.449	1.275	1.617
RMSD($°C$)	1.608	1.643	1.551	1.736
Correlation	0.996	0.997	0.995	0.999

Table 5.1: *Statistics of temperature in the Atlantic Ocean including the Atlantic part of the Southern Ocean.*

	Run 1	Run 2	Run 3	Run 4
Bias($°C$)	0.277	0.332	0.234	0.358
RMSD($°C$)	1.145	1.149	1.141	1.167
Correlation	0.995	0.995	0.995	0.994

Table 5.2: *Statistics of temperature in the Indian and Pacific Oceans, including their Southern Ocean part.*

The changes in the in the sensitivity runs 2 - 4 relative to the standard model did not have a significant change in the statistics of temperature in the Atlantic and Pacific Oceans. This can be seen in Tables 5.1 and 5.2 where the correlation coefficient for the temperature distribution in the Atlantic and Pacific Oceans did not change significantly. Independent of the modifications made, all runs had a strong positive relationship between the sensitivity model runs and the observational data which is the same as the standard model run. The RMSD and biases in the temperature in both the Atlantic and the Pacific also did not show much change. The bias, correlation and RMSD increased slightly in the model runs with decreased diffusivity rate and the shallowed Denmark Strait topography but decreased when the diffusivity rate was increased in both basins. This means the model Run 3 brings temperature distribution in the standard model somewhat closer to the observational data.

	Run 1	Run 2	Run 3	Run 4
Bias	0.523	0.528	0.510	0.558
RMSD	0.595	0.599	0.584	0.628
Correlation	0.735	0.735	0.733	0.739

Table 5.3: *Statistics of salinity in the Atlantic Ocean including the Atlantic part of the Southern Ocean.*

	Run 1	Run 2	Run 3	Run 4
Bias	0.262	0.262	0.265	0.262
RMSD	0.350	0.353	0.350	0.356
Correlation	0.708	0.706	0.714	0.702

Table 5.4: *Statistics of salinity in the Indian Pacific Oceans, including their Southern Ocean part.*

From Tables 5.3 and 5.4, the biases, RMSD and correlation coefficients for salinity distribution in the Atlantic and Pacific Oceans show similar effects of the model modifications as the statistics of the temperature distribution. The bias, correlation and RMSD increased slightly in the model runs with decreased diffusivity rate and the shallowed Denmark Strait topography but decreased when the diffusivity rate was increased. This also confirms why slight differences are seen in Figures 4.2 and 4.4 and Run 3 again brings the salinity in the model closer to the observational data.

The statistics of the nitrate in the Atlantic and Pacific Oceans shows significant changes in the bias, RMSD and correlation coefficient. From Table 5.5 and 5.6, increasing and decreasing the diffusivity rate reduces the biases in the Atlantic and

	Run 1	Run 2	Run 3	Run 4	Run 6	Run 7	Run 8	Run 9
Bias ($\mu molL^{-1}$)	-2.736	-2.574	-2.567	-2.890	-3.411	-3.762	-4.181	-4.943
RMSD ($\mu molL^{-1}$)	7.976	8.019	7.965	7.764	7.799	7.761	7.824	7.932
Correlation	0.754	0.747	0.752	0.773	0.772	0.782	0.785	0.801

Table 5.5: *Statistics of DIN in the Atlantic Ocean including the Atlantic part of the Southern Ocean.*

	Run 1	Run 2	Run 3	Run 4	Run 6	Run 7	Run 8	Run 9
Bias ($\mu molL^{-1}$)	0.913	0.851	0.874	0.943	1.132	1.251	1.363	1.604
RMSD ($\mu molL^{-1}$)	8.293	8.234	8.373	8.123	8.260	8.543	8.196	8.674
Correlation	0.765	0.769	0.757	0.781	0.788	0.791	0.814	0.827

Table 5.6: *Statistics of DIN in the Indian Pacific Oceans, including their Southern Ocean part.*

the Pacific Ocean. Increasing the diffusivity rate reduces the correlation in the Atlantic and the Pacific. But decreasing the diffusivity rate reduces the correlation coefficient in the Atlantic but increases it in the Pacific. Shallowing Denmark Strait topography also increases the bias and the correlation but decreases the RMSD. All the biogeochemical modification model runs generally show an increase in the correlation coefficient and decreases the RMSD but an increase in the bias in both the Atlantic and the Pacific Oceans, with the strongest changes in Run 9.

	Run 1	Run 2	Run 3	Run 4
Bias ($\mu molL^{-1}$)	0.637	0.094	0.831	-4.196
RMSD ($\mu molL^{-1}$)	43.292	43.161	45.537	42.119
Correlation	0.817	0.822	0.820	0.821

Table 5.7: *Statistics of oxygen in the Atlantic Ocean including the Atlantic part of the Southern Ocean.*

For the distribution of oxygen, all the modifications caused a slight increase in the correlation in the Pacific and the Atlantic Ocean. The RMSD was decreased when the diffusivity rate was decreased and topography in the Denmark Strait was shallowed but increased when the diffusivity rate was increased. This means Run 4 gives the overall best agreement in the Atlantic and the Pacific since it gives the lowest RMSD. The bias in the Pacific Ocean was increased when the diffusivity

	Run 1	Run 2	Run 3	Run 4
Bias ($\mu molL^{-1}$)	7.110	7.171	8.580	4.674
RMSD ($\mu molL^{-1}$)	43.610	43.331	44.915	41.780
Correlation	0.765	0.770	0.755	0.779

Table 5.8: *Statistics of oxygen in the Indian and Pacific Ocean, including their Southern Ocean part.*

rate was increased but decreased when the Denmark Strait was shallowed as shown in Tables 5.7 and 5.8. The Atlantic Ocean shows an increase in the bias when the diffusivity rate was increased and the Denmark Strait topography shallowed but highly decreased when the diffusivity constant was was decreased. Run 4, in this case, brings the oxygen in the model closer to the observation both in the Atlantic and Pacific.

The statistics give some contradictory information. From the temperature and salinity, clearly Run 3 is the best. From the nitrate and oxygen, there seems to be a contradiction between bias and correlation. The runs that gave the clearest improvement in the correlation are Run 4 and Run 9. But these generally show higher bias. Nevertheless, given that Run 4 also improves the overturning, we would choose Run 4 and Run 9 as the ones that give the best improvement by changing either the physical and biogeochemical model parametrisation.

Run 4 gives the best improvement in the overturning strength and statistics and Run 9 gives the biggest improvement in the nitrate distribution. The standard run was too warm and salty in the deep Atlantic and Pacific. Run 4 also produced a warmer and saltier Atlantic deep water. This makes it not a good fit for temperature and salinity distribution in the Atlantic and Pacific Oceans as seen in the statistics (low correlation and high RMSD) but one thing is it has an improved overturning strength which is very important in the temperature and salinity distribution.

For the nitrate, the standard model produced a concentration which is too high in the surface and the Southern Ocean and decreases in the deep Atlantic and Pacific waters. In Run 4 there is an increase in the deep waters and a decrease at the surface and the Southern Ocean. This is in the right direction to improve the fit for nitrate distribution in the Atlantic and Pacific Oceans as can be seen in the statistics (low RMSD and high correlation). In the Atlantic, this could be caused by the higher AABW inflow in Run 4, compared with Run 1, which brings higher DIN concentrations. In the Pacific, this may be due to an overall slightly slower overturning which leads to a larger accumulation of remineralised nitrate.

The oxygen concentration in the standard model in the Atlantic and Pacific Oceans shows an increase in the deep waters and decreases at the surface and the Southern Ocean. in Run 4 the oxygen concentration was reduced in the Atlantic and Pacific waters and slightly increased at the surface and the Southern Oceans which is also a fit for the oxygen in the oxygen concentration in the ocean this can be shown in the statistics (low RMSD and slightly high correlation).

For the biogeochemical model parameter changes, since the standard model produced higher nitrates concentration in the surface and the Southern Ocean for both the Atlantic and Pacific, Runs 6 to 9 all shows the an improved since there is a reduction at the surface and slight increases in the deep ocean for the Atlantic and the Pacific oceans. Run 9 gives the best fit as seen in the statistics (low RMSD and higher correlation). This is mostly due to a deepening of remineralisation, which decreases nitrate in the depth around $1000m$ but increases below it. In the Atlantic, the slight decrease in the deep ocean could be driven by a reduction in biological production, due to lower surface nutrients.

Chapter 6

Summary and outlook

The distribution of nitrate and oxygen in the subsurface ocean is regulated by transport and mixing through the ocean circulation, by remineralisation of organic matter and by the amount of nitrate and oxygen in the water mass formation region, which is sometimes named as the 'pre-formed concentration'. As a result the distribution of nutrient reflects both water mass composition, such as in AAIW with high pre-formed nitrate concentration, and water mass age, as reflected in the increase of nitrate from the deep North Atlantic to the deep North Pacific. In biogeochemical modelling, both the representation of the formation and spreading of the water masses and of the remineralisation of sinking organic matter have some imperfections which is reflected in the modelled distribution of nutrients and oxygen.

In this study, first an analysis was made to verify how well the distributions of temperature, salinity, nitrate and oxygen are represented in a global set-up of the REcoM-2 model initialised with fields from the World Ocean Atlas 2009 under climatological atmospheric forcing. The comparison between the REcoM-2 and the observational WOA09 outputs shows some differences. The model produced a temperature and salinity distribution after an integration of over 1000 years that is higher than the observational data in the deep Atlantic and Pacific, which is a common feature in a low resolution models. The model also has a too high oxygen concentration and a too low nutrient concentration in the Atlantic and Pacific deep ocean. In order to rectify the model-data differences, a number of sensitivity studies were performed with the model to find out whether the deviations were due to the physical circulation or the representation of the biological pump.

Shallowing the Denmark Strait topography, decreasing and increasing the diffusivity constant in the GM parametrisation were the parameters changed in physics whereas increasing the vertical gradient of the sinking speed and reducing the remineralisation constant for nitrates and carbon were the changes made in the biogeochemical model.

Some of the changes in the physics and the biogeochemistry result in a clear improvement in the nitrate fields in terms of the biases, correlation and the RMSD of the sensitivity experiments between model output and the WOA09 data. The biases of the DIN were decreased and their correlation was increased. The RMSD was reduced when the vertical gradient of the sinking speed was increased and increased when the carbon and nitrogen remineralisation rate was decreased.

Generally Runs 4 and 9 gave the clearest improvement in the correlation. From the statistics, Run 3 produced the best fit for temperature and salinity fields in the model. Even though Run 4 gave a higher biases, it also lead to a reduction in the strength of the Atlantic overturning circulation to a more realistic value. Run 9 gives the best fit among the changes in the biogeochemical model parametrisation.

This study is still a fairly limited attempts to improve the model-data agreement in this combination of the MITgcm circulation model with the REcoM-2 biogeochemical model. Two model runs of the total of eight that were considered give the best fit to the observational WOA09 data one of them by influencing model circulation, the other by affecting remineralisation, and it would be valuable to combine the two to see the effect. Also we did only a very limited study of the effects of the physical parametrisation here. Another parameter that should be investigated for its effect on the ocean biogeochemistry is for example the cross-isopycnals or vertical diffusivity. The cold bias the mid-depth North Pacific may be an indication that increasing this parameter may improve the model.

Bibliography

Amante, C. & Eakins, B. W. (2009), 'Etopo1 arc-minute global relief model: procedures, data sources and analysis'.

Anderson, L. A. (1995), 'On the hydrogen and oxygen content of marine phytoplankton', *Deep Sea Research Part I: Oceanographic research papers* **42**(9), 1675–1680.

Anderson, L. A. & Sarmiento, J. L. (1994), 'Redfield ratios of remineralization determined by nutrient data analysis', *Global Biogeochemical Cycles* **8**(1), 65–80.

Aumont, O., Orr, J. C., Monfray, P., Madec, G. & Maier-Reimer, E. (1999), 'Nutrient trapping in the equatorial Pacific: The ocean circulation solution', *Global Biogeochemical Cycles* **13**(2), 351–369.

Clarke, R. A. (1984), 'Transport through the cape farewell-femish cap section', *Rapp. PV Reu. Cos. Int. Explor. Mer.* **185**, 120–130.

Colin de Verdière, A. & Ollitrault, M. (2016), 'A direct determination of the World Ocean barotropic circulation', *Journal of Physical Oceanography* **46**(1), 255–273.

Cunningham, S., Alderson, S., King, B. & Brandon, M. (2003), 'Transport and variability of the antarctic circumpolar current in drake passage', *Journal of Geophysical Research: Oceans* **108**(C5).

Ganachaud, A. & Wunsch, C. (2000), 'Improved estimates of global ocean circulation, heat transport and mixing from hydrographic data', *Nature* **408**(6811), 453.

Garcia, H., Locarnini, R., Boyer, T., Antonov, J., Zweng, M., Baranova, O. & Johnson, D. (2010), 'World Ocean Atlas 2009, vol. 4, Nutrients (Phosphate, Nitrate, Silicate), edited by: Levitus, S', *NOAA Atlas NESDIS, US Gov. Printing Office, Wash., DC* **71**.

Geider, R. J., MacIntyre, H. L. & Kana, T. M. (1998), 'A dynamic regulatory model of phytoplanktonic acclimation to light, nutrients, and temperature', *Limnology and Oceanography* **43**(4), 679–694.

Gent, P. R., Willebrand, J., McDougall, T. J. & McWilliams, J. C. (1995), 'Parameterizing eddy-induced tracer transports in ocean circulation models', *Journal of Physical Oceanography* **25**, 463–474.

Hauck, J., Völker, C., Wang, T., Hoppema, M., Losch, M. & Wolf-Gladrow, D. A. (2013), 'Seasonally different carbon flux changes in the Southern Ocean in response to the southern annular mode', *Global Biogeochemical Cycles* **27**(4), 1236–1245.

Hedges, J., Baldock, J., Gélinas, Y., Lee, C., Peterson, M. & Wakeham, S. (2002), 'The biochemical and elemental compositions of marine plankton: A NMR perspective', *Marine Chemistry* **78**(1), 47–63.

Hirose, K. & Kamiya, H. (2003), 'Vertical nutrient distributions in the western North Pacific Ocean: Simple model for estimating nutrient upwelling, export flux and consumption rates', *Journal of Oceanography* **59**(2), 149–161.

Holm-Hansen, O. (1985), Nutrient cycles in antarctic marine ecosystems, *in* 'Antarctic nutrient cycles and food webs', Springer, pp. 6–10.

Imawaki, S., Uchida, H., Ichikawa, H., Fukasawa, M. & Umatani, S.-i. (2001), 'Satellite altimeter monitoring the kuroshio transport south of japan', *Geophysical Research Letters* **28**(1), 17–20.

Johnson, D. R. (2010), 'World Ocean Atlas 2009', *Levitus, Ed. NOAA Atlas NESDIS* **67**.

Jungclaus, J., Fischer, N., Haak, H., Lohmann, K., Marotzke, J., Matei, D., Mikolajewicz, U., Notz, D. & Storch, J. (2013), 'Characteristics of the ocean simulations in the max planck institute ocean model (mpiom) the ocean component of the mpi-earth system model', *Journal of Advances in Modeling Earth Systems* **5**(2), 422–446.

Kanzow, T., Cunningham, S., Johns, W., Hirschi, J. J., Marotzke, J., Baringer, M., Meinen, C., Chidichimo, M., Atkinson, C., Beal, L. et al. (2010), 'Seasonal variability of the Atlantic meridional overturning circulation at 26.5 N', *Journal of Climate* **23**(21), 5678–5698.

Körtzinger, A., Hedges, J. I. & Quay, P. D. (2001), 'Redfield ratios revisited: Removing the biasing effect of anthropogenic CO_2', *Limnology and Oceanography* **46**(4), 964–970.

Kriest, I. & Oschlies, A. (2008), 'On the treatment of particulate organic matter sinking in large-scale models of marine biogeochemical cycles', *Biogeosciences (BG)* **5**, 55–72.

Kriest, I. & Oschlies, A. (2011), 'Numerical effects on organic-matter sedimentation and remineralization in biogeochemical ocean models', *Ocean Modelling* **39**(3), 275 – 283.

Large, W. G. & Yeager, S. (2009), 'The global climatology of an interannually varying air–sea flux data set', *Climate dynamics* **33**(2-3), 341–364.

Locarnini, R., Mishonov, A., Antonov, J., Boyer, T. & Garcia, H. (2010), 'World Ocean Atlas 2009, Volume 1: Temperature. 2010', *NOAA Atlas NESDIS* **68**.

Lohmann, G. (1998), 'The influence of a near-bottom transport parameterization on the sensitivity of the thermohaline circulation', *Journal of Physical Oceanography* **28**(10), 2095–2103.

Lumpkin, R. & Speer, K. (2007), 'Global ocean meridional overturning', *Journal of Physical Oceanography* **37**(10), 2550–2562.

Marshall, J., Adcroft, A., Hill, C., Perelman, L. & Heisey, C. (1997), 'A finite-volume, incompressible Navier Stokes model for studies of the ocean on parallel computers', *Journal of Geophysical Research: Oceans* **102**(C3), 5753–5766.

Martin, J. H., Knauer, G. A., Karl, D. M. & Broenkow, W. W. (1987), 'VERTEX: carbon cycling in the Northeast Pacific', *Deep Sea Research Part A. Oceanographic Research Papers* **34**(2), 267–285.

Nowlin Jr, W. D. & Klinck, J. M. (1986), 'The physics of the antarctic circumpolar current', *Reviews of Geophysics* **24**(3), 469–491.

Passow, U. & Carlson, C. A. (2012), 'The biological pump in a high CO_2 world', *Marine Ecology Progress Series* **470**, 249–272.

Reid Jr, J. L. (1962), 'On circulation, phosphate-phosphorus content, and zooplankton volumes in the upper part of the pacific ocean 1', *Limnology and Oceanography* **7**(3), 287–306.

Rennermalm, A. K., Wood, E. F., Weaver, A. J., Eby, M. & Déry, S. J. (2007), 'Relative sensitivity of the atlantic meridional overturning circulation to river discharge into hudson bay and the arctic ocean', *Journal of Geophysical Research: Biogeosciences* **112**(G4).

Schmittner, A., Chiang, J. C. & Hemming, S. R. (2007), 'Introduction: The ocean's meridional overturning circulation', *Ocean Circulation: Mechanisms and Impacts—Past and Future Changes of Meridional Overturning* pp. 1–4.

Schourup-Kristensen, V., Sidorenko, D., Wolf-Gladrow, D. A. & Völker, C. (2014), 'A skill assessment of the biogeochemical model recom2 coupled to the finite element sea ice–ocean model (fesom 1.3)', *Geoscientific Model Development* **7**(6), 2769–2802.

Sigman, D. & Haug, G. (2003), 'The biological pump in the past', *Treatise on geochemistry* **6**, 625.

Stouffer, R. J., Yin, J., Gregory, J., Dixon, K., Spelman, M., Hurlin, W., Weaver, A., Eby, M., Flato, G., Hasumi, H. et al. (2006), 'Investigating the causes of the response of the thermohaline circulation to past and future climate changes', *Journal of climate* **19**(8), 1365–1387.

Timmermann, R., Brocq, A. L., Deen, T., Domack, E., Dutrieux, P., Galton-Fenzi, B., Hellmer, H., Humbert, A., Jansen, D., Jenkins, A. et al. (2010), 'A consistent data set of antarctic ice sheet topography, cavity geometry, and global bathymetry', *Earth System Science Data* **2**(2), 261–273.

Volk, T. & Hoffert, M. I. (1985), 'Ocean carbon pumps: Analysis of relative strengths and efficiencies in ocean-driven atmospheric CO_2 changes', *The Carbon Cycle and Atmospheric CO_2: Natural Variations, Archean to Present* pp. 99–110.

Whitworth III, T. & Peterson, R. (1985), 'Volume transport of the antarctic circumpolar current from bottom pressure measurements', *Journal of Physical Oceanography* **15**(6), 810–816.

Willebrand, J., Barnier, B., Böning, C. W., Dieterich, C., Killworth, P. D., Le Provost, C., Jia, Y., Molines, J.-M. & New, A. L. (2001), 'Circulation characteristics in three eddy-permitting models of the North Atlantic', *Progress in Oceanography* **48**(2-3), 123–161.